AFRL-AFOSR-UK-TR-2024-0018

Multiscale materials science: a mathematical approach to defects

Le Bris, Claude
ECOLE NATIONALE DES PONTS ET CHAUSSEES
CITE DESCARTES
6 AVENUE BLAISE PASCAL
CHAMPS SUR MARNE, , 77420
FRA

01/24/2024
Final Technical Report

Air Force Research Laboratory
Air Force Office of Scientific Research
European Office of Aerospace Research and Development
Unit 4515 Box 14, APO AE 09421

REPORT DOCUMENTATION PAGE

PLEASE DO NOT RETURN YOUR FORM TO THE ABOVE ORGANIZATION.

1. REPORT DATE	2. REPORT TYPE	3. DATES COVERED	
20240124	Final	START DATE 20200930	END DATE 20230929

4. TITLE AND SUBTITLE
Multiscale materials science: a mathematical approach to defects

5a. CONTRACT NUMBER	5b. GRANT NUMBER	5c. PROGRAM ELEMENT NUMBER
	FA8655-20-1-7043	
5d. PROJECT NUMBER	**5e. TASK NUMBER**	**5f. WORK UNIT NUMBER**

6. AUTHOR(S)
Claude Le Bris

7. PERFORMING ORGANIZATION NAME(S) AND ADDRESS(ES)
ECOLE NATIONALE DES PONTS ET CHAUSSEES
CITE DESCARTES
6 AVENUE BLAISE PASCAL
CHAMPS SUR MARNE 77420
FRA

8. PERFORMING ORGANIZATION REPORT NUMBER

9. SPONSORING/MONITORING AGENCY NAME(S) AND ADDRESS(ES)	10. SPONSOR/MONITOR'S ACRONYM(S)	11. SPONSOR/MONITOR'S REPORT NUMBER(S)
EOARD UNIT 4515 APO AE 09421-4515	AFRL/AFOSR IOE	AFRL-AFOSR-UK-TR-2024-0018

12. DISTRIBUTION/AVAILABILITY STATEMENT
A Distribution Unlimited: PB Public Release

13. SUPPLEMENTARY NOTES

14. ABSTRACT
The works reported on here have been performed by Claude Le Bris (PI), Frédéric Legoll (Co- PI), and -- for the work described in Section 2, by Amandine Boucart, a postdoctoral student who joined the team in April 2023 and is funded by ONR. -- for the work described in Section
3, by Rutger Biezemans, a PhD student in the team who defended his thesis in September 2023 and was funded by a fellowship of the Paris Region. -- for the work described in Section 4, by Simon Ruget, who started his PhD in the team in October 2022, and the fellowship of
whom is funded by Inria. -- for the work described in Section 5, by Alberic Lefort, who started his PhD in the team in November 2022. His PhD fellowship is partly funded by this EOARD contract. The works reported on in Sections 3 and 4, although not supported by EOARD, are
part of the global research effort of the team and are closely related to the research performed in the context of the present contract. Sections 2, 4 and 5 collect at their end some perspectives. We hope to proceed with them (subject to EOARD approval of course) in the context of a renewed funding, as proposed in our 2023 white paper. This report is articulated as follows. First, during the funding period, two textbooks on Homogenization Theory havebeen written, and we explain the motivation for this in Section 1.

15. SUBJECT TERMS

16. SECURITY CLASSIFICATION OF:			17. LIMITATION OF ABSTRACT	18. NUMBER OF PAGES
a. REPORT	b. ABSTRACT	c. THIS PAGE		
U	U	U	SAR	50

19a. NAME OF RESPONSIBLE PERSON	19b. PHONE NUMBER *(Include area code)*
DAVID SWANSON	314 235 6001

Standard Form 298 (Rev.5/2020)
Prescribed by ANSI Std. Z39.18

Contract FA 8655-20-1-7043

Multiscale materials science: a mathematical approach to defects

Report 2023 to the European Office of Aerospace Research and Development (EOARD)

C. Le Bris and F. Legoll

October 2022 – September 2023

Contents

Executive Summary

We report here on the work performed during the third year (October 2022 - September 2023) of the contract FA 8655-20-1-7043 on *Multiscale materials science: a mathematical approach to defects*.

The presence of numerous length-scales in material science problems represents a daunting challenge for numerical simulation. Quantifying the effects of defects, and more generally any uncertainty arising from the data, the discretization and the mechanical model has become an increasingly important aspect of multiscale analysis. Such studies open the way to assessing the effective global and local behaviors of materials.

The bottom line of this long-term project, supported by several EOARD funding periods in a row (and conducted in relation to a similar and connected research effort supported by ONR), is to develop new mathematical and numerical tools to address the current challenging problems of interest in materials science. It is our belief that a satisfactory theoretical understanding of ideal *perfect* materials has now been achieved along with the design of reasonably efficient numerical approaches for the simulation of those. It is however a pending challenge to understand, model, simulate and control *real* materials in all their inevitable imperfections. For instance, issues such as the modeling of defects are not so well understood. For this specific funding period, we have studied, both from a theoretical and a numerical perspectives, *equations other than the diffusion equation*. The latter equation has been the common denominator and the main object under consideration for all our previous funding periods. It has been a test-bed for new ideas regarding modeling of defects and uncertainties in the idealized materials, in order to bridge the gap between ideal materials and actual materials. It was now time to begin the adaptation of the mathematical studies and the numerical approaches developed on the case of the diffusion equation to the many other equations that are relevant in the engineering sciences. This is what we are going to describe in the current report, thereby *opening perspectives which are entirely new* in comparison to the past funding periods, which extended from 2009 to 2020. In that spirit, and as explained below, Section 2 is dedicated to fully hyperbolic equations, while Section 5 is dedicated to multiscale reaction-diffusion problems, which hence include a reaction term in addition to the diffusive term.

The works reported on here have been performed by Claude Le Bris (PI), Frédéric Legoll (Co-PI), and

- for the work described in Section 2, by Amandine Boucart, a postdoctoral student who joined the team in April 2023 and is funded by ONR.

- for the work described in Section 3, by Rutger Biezemans, a PhD student in the team who defended his thesis in September 2023 (see [B-PhD]) and was funded by a fellowship of the Paris Region.

- for the work described in Section 4, by Simon Ruget, who started his PhD in the team in October 2022 (see [R-PhD]), and the fellowship of whom is funded by Inria.

- for the work described in Section 5, by Alberic Lefort, who started his PhD in the team in November 2022 (see [L-PhD]). His PhD fellowship is partly funded by this EOARD contract.

The works reported on in Sections 3 and 4, although not supported by EOARD, are part of the global research effort of the team and are closely related to the research performed in the context of the present contract.

Sections 2, 4 and 5 collect at their end some perspectives. We hope to proceed with them (subject to EOARD approval of course) in the context of a renewed funding, as proposed in our 2023 white paper [EOARD-WP].

This report is articulated as follows. First, during the funding period, two textbooks on Homogenization Theory have been written, and we explain the motivation for this in Section 1. This action testifies to our wish to reach the largest possible audience and introduce them to the challenging field of multiscale science.

Second, during the past funding period, we began to consider a whole new set of (multiscale) equations, modeling physical phenomena different from pure diffusion. In that direction, we first investigated *advection-diffusion equations* in the regime when advection dominates diffusion (see our previous report [EOARD-2021]). In spite of its formal proximity with the diffusion equation, the advection-diffusion equation is already remote theoretically since, in sharp contrast to the diffusion equation, it is not self-adjoint. Taking one step further, we focused on the numerical approach for some *fully nonlinear* PDE, namely *Hamilton-Jacobi* equations (see e.g. [ALB23]). Intrigued by this first set of exploratory works on non-diffusive regimes, we have recently started to consider *fully hyperbolic equations*. We report on these preliminary works in Section 2.

In Section 3 of this report, we explain how Multiscale Finite Element methods (MsFEM) can be implemented in a non-intrusive manner. We recall that Multiscale Finite Element Methods are finite element type approaches dedicated to multiscale problems. They first compute local, oscillatory, *problem-dependent* basis functions

which generate a *specific* discretization space, and next perform a Galerkin approximation of the problem on that space. We describe in Section 3 how these approaches can be implemented in a non-intrusive way, in order to facilitate their dissemination within industrial codes or non academic environments.

In Section 4 of this report, we describe some works related to the construction of coarse approximations for problems with highly oscillatory coefficients. This is an idea that we have already studied in the case of a diffusion equation with highly oscillatory diffusion coefficients $A^\varepsilon(x)$ (see [14, 15]). Our aim was to define and construct the best non-oscillating coefficient $\overline{A}$ (think e.g. of a constant coefficient) that was consistent with the behavior of a heterogeneous material modeled by a given highly oscillatory coefficient $A^\varepsilon(x)$. Here, we revisit this question in the setting of Schrödinger equations with rapidly oscillating potentials, using our earlier developments to guide the current work.

The approach we have introduced in [14, 15] can be considered as an alternative pathway to standard homogenization techniques when the latter are difficult to use in practice, in particular when information is missing on the oscillatory potential. It can also be understood as an inverse problem approach: we design a procedure which, using some observations (here the solutions to the highly oscillatory equation for several right-hand sides), identifies the best effective constant potential such that the coarse model using that effective potential is as close as possible to the highly oscillatory Schrödinger model. We have already discussed this problem in our previous report [EOARD-2022], where we have collected some theoretical results and some illustrating numerical results in the one-dimensional setting. In this report (see Section 4), we present a complete numerical investigation of the approach in a *multi-dimensional setting*.

We eventually consider a multiscale time-dependent reaction-diffusion problem (see Section 5), a setting that we have already discussed in our 2022 report [EOARD-2022], where we identified the homogenized limit of the problem. Here, we address the problem from a numerical perspective. The difficulty stems from the fact that, besides the fact that the coefficients of the equation (and therefore the solution) oscillate at a small spacial scale, the problem is also stiff in time. In order to not address all difficulties at the same time, we consider here the eigenvalue variant of the problem, which allows us to leave aside the stiffness in time difficulty. There are two motivations for considering this eigenvalue problem: (i) it can be considered as a first step towards the corresponding time-dependent version of the problem, and (ii) it appears in several applied fields (including neutronics) and is thus interesting in its own right. We note that this problem is different from the equations we have studied in the previous

funding periods by the fact that it is an *eigenvalue* problem and that it includes a *reaction term* (in addition to the diffusive term).

We recall first the homogenized limit of the eigenvalue problem before turning to the construction of MsFEM-type multiscale approaches in the one-dimensional setting. We also present some preliminary results in a multi-dimensional setting.

We acknowledge that the support of EOARD has allowed, in a broad sense, to reinforce the general activity of our group on multiscale methods. We have been able to attract excellent postdoctoral students (for the current reporting period, Amandine Boucart) and PhD students (for the current reporting period, Rutger Biezemans [B-PhD], Rémi Goudey [G-PhD], Alberic Lefort [L-PhD] and Simon Ruget [R-PhD]) in our group, one of them (Alberic Lefort) being funded by this EOARD contract and another one (Amandine Boucart) being funded by ONR. Two PhD students, Rutger Biezemans and Rémi Goudey, have defended their thesis within the current reporting period.

The support of EOARD has also allowed us to develop new or strengthen existing collaborations. First, we have had many discussions with our long term collaborator Alexei Lozinski (University of Besançon), in particular in relation with the PhD of Rutger Biezemans, the supervisors of whom were Claude Le Bris and Alexei Lozinski. Second, during the past years, we have had many exchanges with the group of Daniel Peterseim (University of Augburg). This has led in particular to the organization of two joint workshops on multiscale problems, one in June 2020[1] and one in September 2021[2]. Our specific research activity on MsFEM type approaches has been increasingly intensive in the past years and this continued research effort funded by EOARD has enhanced our visibility at the international level. We are now following up on this upon developping a whole network of domestic and international interactions. Preliminary contacts have been established with several researchers, including Guillaume Enchéry (IFPEn, the French institute for reservoir simulation), Pascal Omnes (CEA, the French nuclear agency), Barbara Verfürth (Bonn university) and Karen Veroy-Grepl (Eindhoven University), on what could be possible tracks for joint research efforts.

[1] see https://www.uni-augsburg.de/de/fakultaet/mntf/math/prof/numa/gamm-fa/french-german-multiscale-workshop/

[2] see https://sites.google.com/view/multiscale2021

References authored by the investigators and their students in the context of the contract[3]

[BLBL24] A. Boucart, C. Le Bris and F. Legoll, work in preparation.

[EOARD-2021] C. Le Bris and F. Legoll, *Multiscale materials science: a mathematical approach to defects*, EOARD Report 2021.

[EOARD-2022] C. Le Bris and F. Legoll, *Multiscale materials science: a mathematical approach to defects*, EOARD Report 2022.

[EOARD-WP] C. Le Bris and F. Legoll, *Mathematical approaches to some hyperbolic problems in multiscale materials science*, White Paper to EOARD, 2023.

Articles in peer-reviewed journals:

The support of EOARD has been explicitly acknowledged in all the following publications:

[ALB23] Y. Achdou and C. Le Bris, *Homogenization of some periodic Hamilton-Jacobi equations with defects*, Communications in P.D.E., 48(6):944–986, 2023.

[BLBLL23a] R. Biezemans, C. Le Bris, F. Legoll and A. Lozinski, *Non-intrusive implementation of Multiscale Finite Element Methods: an illustrative example*, J. Comput. Phys., 477, article 111914, 2023.

[BLBLL23b] R. Biezemans, C. Le Bris, F. Legoll and A. Lozinski, *Non-intrusive implementation of a wide variety of Multiscale Finite Element Methods*, Comptes Rendus Mécanique, 351(1), online first, 2023.

[BLB23a] X. Blanc and C. Le Bris, *Homogénéisation en milieu périodique . . . ou non: une introduction*, Maths & Applications, vol. 88, Springer, 2023.

[BLB23b] X. Blanc and C. Le Bris, *Homogenization theory for multiscale problems: an introduction*, MS&A, Modeling, Simulation and Applications, vol. 21, Springer, 2023.

[3] We collect here references corresponding to works submitted or published during the third year of this contract. Works that are not related to the contract but are relevant to this report are cited at the end of this document.

[CL23] L. Chamoin and F. Legoll, *An introductory review on a posteriori error estimation in Finite Element computations*, SIAM Review, 65(4):963–1028, 2023.

[GLB23] R. Goudey and C. Le Bris, *Linear elliptic homogenization for a class of highly oscillating non-periodic potentials*, arxiv preprint 2205.15600 (available at https://arxiv.org/abs/2205.15600), to appear in SIAM J. Math. Anal.

[L22] C. Le Bris, *Defects in homogenization theory*, Séminaire Laurent Schwartz, EDP et Applications, année 2022-2023, Exposé II (18 octobre 2022), 1–16.

PhD thesis and other articles:

[B-PhD] R. Biezemans, *Multiscale methods: non-intrusive implementation, advection-dominated problems and related topics*, PhD thesis, defended on September 21, 2023.

[G-PhD] R. Goudey, *Homogenization problems in the presence of defects*, PhD thesis, defended on October 10, 2022 (available at https://pastel.hal.science/tel-04010195v1).

[L-PhD] A. Lefort, *Multiscale numerical methods for reaction-diffusion equations*, PhD thesis, in preparation (defense expected Summer 2025).

[R-PhD] S. Ruget, *On the construction of coarse approximations for Schrödinger-type problems with highly oscillatory coefficients*, PhD thesis, in preparation (defense expected Summer 2025).

Conference presentations:

[c-B23a] R. Biezemans, *Non-intrusive implementation of multiscale finite element methods*, SIAM CSE conference, Amsterdam, February 2023.

[c-B23b] R. Biezemans, *Improved multiscale finite element methods for advection-diffusion problems*, Computational Fluids Conference, Cannes, April 2023.

[c-LB23a] C. Le Bris, *Defects in homogenization theory*, Oberseminar Analysis – Probability, Leipzig, January 2023.

[c-LB23b] C. Le Bris, *Defects in homogenization theory and related issues: Materials science and multiscale computational approaches*, Numerical Analysis seminar of the Department of Mathematics of the University of Hong Kong, February 2023 (online talk).

[c-LB23c] C. Le Bris, *Méthodes d'éléments finis multi-échelles: enjeux, succès et questions en suspens*, Collège de France seminar, Paris, March 2023 (recording available at https://www.college-de-france.fr/fr/agenda/seminaire/mathematiques-appliquees/methodes-elements-finis-multi-echelles-enjeux-succes-et-questions-en-suspens).

[c-L22] F. Legoll, *Multiscale Finite Element Methods for advection-diffusion problems*, Numerical Analysis seminar of the Department of Mathematics of the University of Hong Kong, October 2022 (online talk).

[c-L23a] F. Legoll, *Multiscale Finite Element approaches: Error estimations and adaptivity for an enriched variant*, ADMOS Conference, Goteborg, June 2023.

[c-L23b] F. Legoll, *Variance reduction methods in random homogenization by using surrogate models*, ICIAM conference, Tokyo, August 2023 (online talk).

[c-L23c] F. Legoll, *Multiscale Finite Element Methods for advection-diffusion problems*, EnuMath conference, Lisbon, September 2023.

[c-L23d] F. Legoll, *Multiscale Finite Element Methods for heterogeneous plates*, ComPlas conference, Barcelona, September 2023.

[c-R23] S. Ruget, *Construction of coarse approximations for a Schrödinger problem with highly oscillatory coefficients* (poster), Congrès des Jeunes Chercheurs en Mathématiques et Applications, Saclay, September 2023.

1 Publication of two books

During the funding period, Claude Le Bris has co-authored (with Xavier Blanc, Université Paris-Cité) two textbooks on Homogenization Theory, one in French [BLB23a] and one in English [BLB23b]. The two books mostly present the same material. The French version however dwells a bit more into the theoretical aspects while the English version is slightly more into computational issues.

As exposed in the foreword of the books, the common motivation for the two textbooks was the following.

Homogenization theory was born fifty years ago and has generated many offsprings. It has emerged at the interface between an abstract viewpoint and practical considerations in the specific context of periodic media. It was then increasingly considered for other media: locally periodic media, random media, etc. It was originally considered for linear equations. It now applies to semilinear equations, quasilinear equations such as the p-Laplacian, and even fully nonlinear equations, such as the Hamilton-Jacobi equations. It initially provided a mean to change scale in the bulk of a domain. It then became a manner to study boundary layers and derive wall laws. After addressing only equations, such as the diffusion equation, it was next applied to *systems of equations*, such as the Stokes system. Over the years, it has also addressed spectral problems and not only problems for a given right-hand side, time-dependent problems after steady-state problems, problems posed over perforated domains or domains that have fractal boundaries rather than problems posed on nice and regular domains.

That said, such a mature mathematical theory runs a twofold risk. The first risk is that the theoretical developments become too technical. Most of the simple questions have essentially been solved. Those that remain unsolved are challenging. They require an exceptional creativity and an elaborate technical toolbox. Several recent contributions in the area are extremely technical and their mathematical substance may escape the outsider. If the sophistication may be an incentive for some readers, it might also act as a repellent for some other readers. The second risk is that the theoretical developments, although originally motivated by applications, progressively get somewhat disconnected from reality.

We therefore believed it was time to summarize the essence of the theory and make it accessible to outsiders. Major reference treatises exist. Other monographs also complement the above treatises by focusing on some given aspects or some given approaches. Some research books aim at presenting new developments, some didactic and pedagogic presentations initiate the readers to elaborate techniques. We thought that another book of introduction to the topic could help. It could usefully complement

the already existing literature, providing a different perspective or a different take on the various issues. The student, or the outsider to the field, may then cherry pick which pedagogic presentation fits best with their own perception or allows for the most efficient learning curve.

It was also ample time to reconcile homogenization theory with its original practical objectives. As we mentioned above, the development of homogenization theory stemmed from practical questions, for instance the wish to better understand various questions arising in material sciences such as phase transitions, mixing properties, etc. The success of the theory has been substantial, both in terms of phenomenological understanding and in terms of theoretical equipment. Homogenization theory has also been useful quantitatively. In its modern variant known as *multiscale methods*, it serves as a theoretical guideline. It provides the necessary theoretical understanding of numerous computational approaches that address various situations. In many actual circumstances, practitioners need a quick and quantitative answer to the questions they have. What if the actual material does not satisfy the idealized assumptions of the theory? One must proceed no matter what. How? What macroscopic properties to expect? The mathematical apparatus provided by classical homogenization theory may then be very frustrating. A practitioner in an industrial context may typically be able to only allocate at most a couple of hours of computational time for the simulation. An approximate quantitative reply is nevertheless expected. At least the order of magnitude of the reply must be correct, or the trend to be anticipated if a change is being operated in the conditions of the experiments or the parameters of the industrial device. It is then unclear how to change the focus, from a theory that primarily aims at accuracy to a methodology that provides coarse but swift replies.

We also aimed at revisiting a series of past contributions (over two decades, and essentially all partly supported by our continued funding at EOARD and ONR) performed under the leadership of and in collaboration with Pierre-Louis Lions, that have led us to develop a portfolio of modeling strategies on *nonperiodic* problems and approaches. We thus revisited in the books a portion of homogenization theory through the prism of a large variety of nonperiodic problems, all arising from practical considerations.

The French version of the book has been published in March 2023, and the English version in April. At the time of writing of this report, they have been downloaded about 700 and 1,200 times, respectively.

2 Multiscale hyperbolic problems

[Work expanded in [BLBL24]].

In line with the idea, outlined in the Executive Summary, to study heterogeneous equations that are less and less elliptic and more and more hyperbolic in nature, we have recently started to investigate multiscale *conservation laws*. This work is performed in the context of the postdoctoral fellowship of Amandine Boucart, funded by ONR.

The prototypical (multiscale) hyperbolic equation that we have considered is

$$\frac{\partial u_\varepsilon}{\partial t} - \varepsilon\,\Delta u_\varepsilon + \operatorname{div} F\left(\frac{x}{\varepsilon}, u_\varepsilon\right) = 0 \tag{1}$$

for ε small, where u_ε is a scalar-valued function and the so-called *flux* F is a vector-valued function, supposedly depending upon the small scale ε. The equation is supplied with an initial condition, and possibly boundary conditions.

Since the flux varies at the scale ε, it is well known that obtaining an accurate approximation of u_ε requires a small discretization step, if using standard approaches. The number of degrees of freedom is then very large. This leads to a usually prohibitive computational complexity. As is usual for multiscale problems, a first strategy is to theoretically identify the limit $u^\star$ of u_ε when $\varepsilon \to 0$, and build a numerical approach to approximate $u^\star$. This is the realm of homogenization theory. We describe in Section 2.1 the homogenized limit of (1), and next present in Section 2.2 our numerical investigations on this problem. Perspectives are collected in Section 2.3. We note that, to the best of our knowledge, the work we describe below is the first to introduce a numerical approach, based on periodic homogenization theory, in the specific context of conservation laws.

2.1 Homogenized limit

The homogenized limit of (1) has been identified in [6] in the periodic setting. We thus assume that, for any $p \in \mathbb{R}$, the function $y \mapsto F(y,p)$ is periodic. We restrict our presentation to the case when the function $v \mapsto F(y,v)$ is linear, i.e.

$$F(y,v) = v\,b(y)$$

for some vector-valued, periodic function $y \mapsto b(y)$, although [6] actually considers both linear and nonlinear cases. In the linear setting, the oscillatory problem (1) is

$$\frac{\partial u_\varepsilon}{\partial t} - \varepsilon\,\Delta u_\varepsilon + \operatorname{div}\left[u_\varepsilon\, b\left(\frac{x}{\varepsilon}\right)\right] = 0. \tag{2}$$

As is usual in homogenization, we introduce a corrector problem, which reads here as follows: find the zero-mean periodic function w solution to

$$-\Delta_y w(y) + \mathrm{div}_y \left[(1 + w(y))\, b(y) \right] = 0. \tag{3}$$

We next introduce the homogenized flux defined, for any $p \in \mathbb{R}$, by

$$F^\star(p) = p \int_Q (1 + w(y))\, b(y)\, dy,$$

where Q is of course the periodic cell. We can write $F^\star$ in the form $F^\star(p) = p\, b^\star$ for some homogenized advection vector $b^\star$ given by

$$b^\star = \int_Q (1 + w(y))\, b(y)\, dy. \tag{4}$$

For any function $u^0 : \mathbb{R}^d \to \mathbb{R}$ (which plays the role of an initial condition), consider the oscillatory problem (2) posed in $\mathbb{R}^d$ and complemented with the initial condition

$$u_\varepsilon(t = 0, x) = u^0(x) \left[1 + w\left(\frac{x}{\varepsilon} \right) \right]. \tag{5}$$

In the terminology of such problems, this initial condition is said to be well-prepared, in the sense that it is oscillatory in space and that its fine-scale oscillations are *exactly* given by the corrector function.

Consider now the homogenized problem

$$\frac{\partial u^\star}{\partial t} + \mathrm{div} \left[u^\star\, b^\star \right] = 0, \tag{6}$$

complemented with the initial condition $u^\star(t = 0, x) = u^0(x)$.

As stated in [6], the homogenization result is that the difference $u_\varepsilon(t, x) - u_{\varepsilon,1}(t, x)$ goes to zero when $\varepsilon \to 0$, in an appropriate strong norm, where the reconstructed approximation $u_{\varepsilon,1}$ is defined by

$$u_{\varepsilon,1}(t, x) = u^\star(t, x) \left[1 + w\left(\frac{x}{\varepsilon} \right) \right]. \tag{7}$$

2.2 Numerical investigations

We have numerically investigated the linear oscillatory problem (2) in the two-dimensional context, with the choice

$$b(y_1, y_2) = \begin{pmatrix} 1 + \sin(2\pi\, y_1) \\ 2 - \cos(2\pi\, y_2) \end{pmatrix},$$

which is indeed Q-periodic, with $Q = (0,1)^2$.

Our aim here, while considering a simple linear and periodic problem, is to numerically investigate the accuracy of the approximation (7) provided by homogenization theory. We see this work as a proof of concept that homogenization results can be put in practice in a useful manner. We will then be in position to address more complicated situations, as described in the perspectives collected in Section 2.3.

2.2.1 Corrector problem

We first need to solve the corrector problem (3). This problem is elliptic and can be solved using a standard Finite Element technique (in practice, we use a P1 discretization of the periodic cell Q with a mesh of size $h_Q = 1/50$). We can next compute $b^\star$ given by (4), and we have found

$$b^\star \approx \begin{pmatrix} 0.988 \\ 1.98 \end{pmatrix}.$$

We emphasize that our choice of b leads to a homogenized advection vector $b^\star$ which is neither along the horizontal, not the vertical direction. The homogenized problem (6) is thus genuinely two-dimensional.

2.2.2 Oscillatory problem

We are now in position to introduce a reference numerical approach to discretize the oscillatory problem (2) with the well-prepared initial condition (5). To that aim, we first need to restrict the problem (2) on a bounded domain Ω, and we choose to work on $\Omega = (0,1)^2$. We then complement (2) with periodic boundary conditions on $\partial\Omega$, to remain as close as possible to the theoretical setting investigated in [6]. To define the initial condition (5), we choose

$$u^0(x_1, x_2) = \cos(2\pi\, x_1)\, \sin(2\pi\, x_2). \tag{8}$$

This function is shown on Figure 3 below. We show on Figure 1 the initial condition $u_\varepsilon(t = 0)$ defined by (5) for two values of ε (we have been careful to choose values of ε such that the initial condition $u_\varepsilon(t = 0)$ satisfies periodic boundary conditions on $\partial\Omega$, in accordance with our choice to complement the oscillatory problem (2) on Ω by periodic boundary conditions). As expected, we observe that, when ε becomes smaller, the period of the oscillations present in $u_\varepsilon(t = 0)$ becomes smaller.

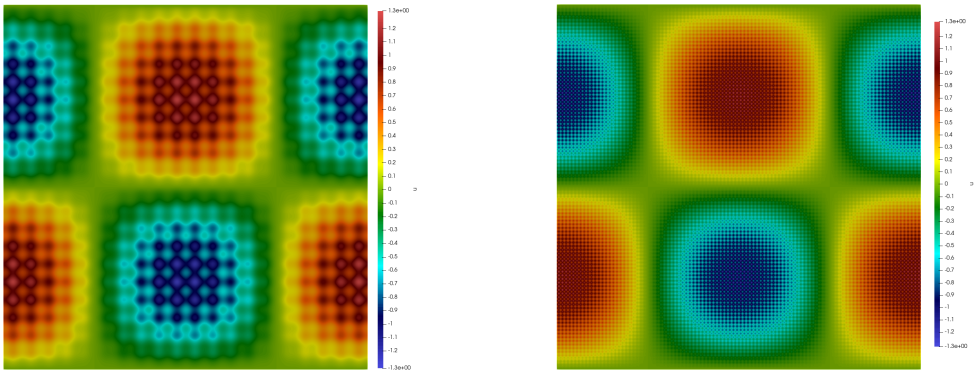

Figure 1 – Representation of the initial condition $u_\varepsilon(t=0)$ defined by (5), for different values of ε (left: $\varepsilon = 0.05$; right: $\varepsilon = 0.01$).

Since the problem (2) is parabolic, it can be discretized by a finite element method. Since the advection field is oscillatory, it is natural to consider a mesh size h much smaller than the oscillation period ε, namely $h \ll \varepsilon$. In practice, we choose $h = 0.003$ when $\varepsilon = 0.05$ (resp. $h = 0.002$ when $\varepsilon = 0.01$), which ensures that $h/\varepsilon \approx 1/20$ for the first case and $h/\varepsilon = 1/5$ for the last case.

We adopt the following discretization strategy for (2). We consider an implicit Euler time-scheme,

$$\frac{u^{n+1}}{\Delta t} - \varepsilon\,\Delta u^{n+1} + \mathrm{div}\left[u^{n+1}\,b\left(\frac{x}{\varepsilon}\right)\right] = \frac{u^n}{\Delta t}, \tag{9}$$

where u^n is the approximation of $u_\varepsilon(t_n,\cdot)$ at time $t_n = n\,\Delta t$. In practice, we work with the time step $\Delta t = \dfrac{1}{2}\,\dfrac{h}{\sqrt{2}\sqrt{(b_1^\star)^2+(b_2^\star)^2}}$, where $b^\star = \begin{pmatrix} b_1^\star \\ b_2^\star \end{pmatrix}$ is the homogenized advection field and h is the mesh size (note that Δt depends on ε since h depends on ε). The variational formulation of (9) is to look for $u^{n+1} \in H^1_{\mathrm{per}}(\Omega)$ such that, for any $v \in H^1_{\mathrm{per}}(\Omega)$,

$$\frac{1}{\Delta t}\int_\Omega u^{n+1}\,v + \varepsilon\int_\Omega \nabla u^{n+1}\cdot\nabla v - \int_\Omega u^{n+1}\,b\left(\frac{x}{\varepsilon}\right)\cdot\nabla v = \frac{1}{\Delta t}\int_\Omega u^n\,v, \tag{10}$$

where we have performed an integration by parts in the last term of the left-hand side and used that $x \mapsto b(x/\varepsilon)$ is periodic on Ω (the boundary term thus vanishes in the integration by parts), a consequence of the specific values of ε that we have considered. The variational formulation (10) is next discretized by a Galerkin approximation on piecewise affine functions on the mesh $\mathcal{T}_h$.

We show on Figure 2 the reference solution u_ε at the time $T = 0.2$, for the same two values of ε as on Figure 1. As expected, we observe that, when ε becomes smaller, the period of the oscillations of $u_\varepsilon(T, \cdot)$ become smaller.

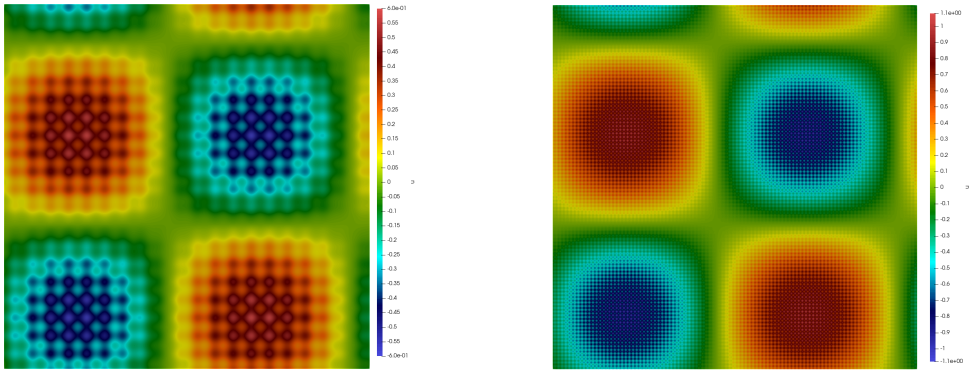

Figure 2 – Representation of the reference solution u_ε at time $T = 0.2$, for different values of ε (left: $\varepsilon = 0.05$; right: $\varepsilon = 0.01$).

2.2.3 Homogenized problem

We eventually turn to the discretization of the homogenized problem (6). In general, the homogenized problem is a conservation law, and we thus adopt a finite volume approach to discretize it. In line with our choice for the oscillatory problem (2), we here complement (6) with periodic boundary conditions.

To discretize (6), we use the Lax-Wendroff scheme. In the two-dimensional case, there are several ways to write such a scheme. The one we adopt here has been proposed in [7] and reads, for the general problem $\dfrac{\partial v}{\partial t} + \operatorname{div} \mathcal{F}(v) = 0$ with $\mathcal{F}(v) = \begin{pmatrix} F(v) \\ G(v) \end{pmatrix} = v \begin{pmatrix} b_1 \\ b_2 \end{pmatrix}$, as the conservative scheme

$$\frac{v_{i,j}^{n+1} - v_{i,j}^n}{\Delta t} + \frac{F_{i+1/2,j}^n - F_{i-1/2,j}^n}{\Delta x} + \frac{G_{i,j+1/2}^n - G_{i,j-1/2}^n}{\Delta y} = 0$$

with

$$F_{i-1/2,j}^n = \frac{F(v_{i-1,j}^n) + F(v_{i,j}^n)}{2} - \frac{b_1 \, (b_1 + b_2) \, \Delta t}{2\Delta x} \, (v_{i,j}^n - p \, v_{i-1,j}^n - q \, v_{i,j-1}^n),$$
$$G_{i,j-1/2}^n = \frac{G(v_{i,j-1}^n) + G(v_{i,j}^n)}{2} - \frac{b_2 \, (b_1 + b_2) \, \Delta t}{2\Delta y} \, (v_{i,j}^n - p \, v_{i-1,j}^n - q \, v_{i,j-1}^n),$$

where the parameters p and q are given by $p = \dfrac{b_1}{b_1 + b_2}$ and $q = \dfrac{b_2}{b_1 + b_2} = 1 - p$.

Since the homogenized problem is a constant coefficient problem, it is possible to use a larger cell size Δx than when discretizing the oscillatory problem. Here, for the sake of comparing the reference solution with the homogenized solution without adding any coarse discretization error, we use essentially the same discretization parameters for both problems. The oscillatory problem is discretized in space using a finite element method based on a mesh $\mathcal{T}_h$ made of isosceles right triangles (we mesh Ω by squares and next cut them in half), and we thus solve the homogenized problem by a finite volume method based on square elements, each of which being the union of two mesh triangles of $\mathcal{T}_h$. We thus take $\Delta x = \Delta y = h$. In order to satisfy the CFL condition, we use the time step $\Delta t = \dfrac{1}{2} \dfrac{h}{\sqrt{2}\sqrt{(b_1^\star)^2 + (b_2^\star)^2}}$.

We show on Figure 3 the initial condition of the homogenized problem (namely u^0 given by (8)) and the homogenized solution $u^\star$ at the time $T = 0.2$. We observe that the scheme is very accurate. The function has simply been transported in the direction of $b^\star$. We see that the time $T = 0.2$ is sufficiently large to observe (at the scale of Figure 3) a transport of the initial condition (the functions at $t = 0$ and $t = T$ do not lie on top of each other).

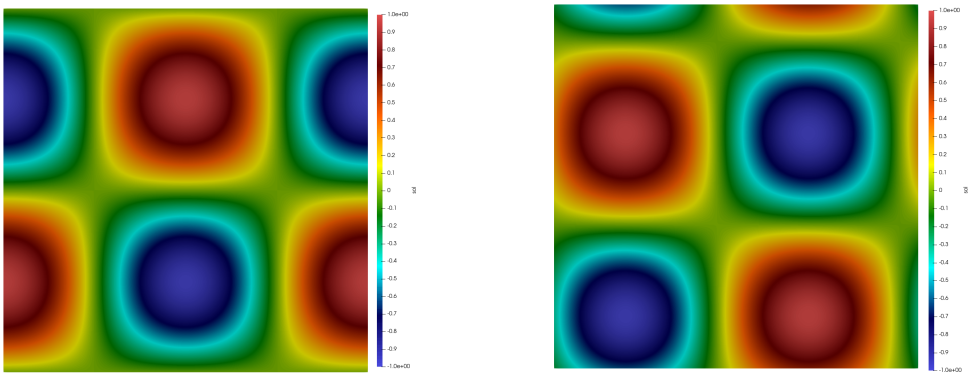

Figure 3 – Representation of the homogenized solution $u^\star$: initial condition (left) and solution at time $T = 0.2$ (right). Two sets of discretization parameters can be used (for the two different values of ε we have considered for the reference solution); at the scale of the figure, the two approximations are indistinguishable.

2.2.4 Errors

We show on Figure 4 the reconstructed approximation $u_{\varepsilon,1}$ (defined by (7)) at the time $T = 0.2$, for the two values of ε that we have considered.

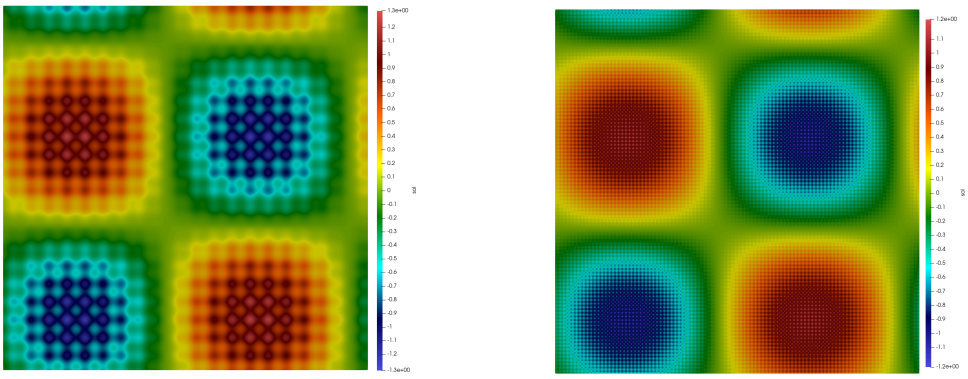

Figure 4 – Representation of the reconstructed approximation $u_{\varepsilon,1}$ at time $T = 0.2$, for different values of ε (left: $\varepsilon = 0.05$; right: $\varepsilon = 0.01$).

We are eventually in position to compute the difference between the reference solution u_ε and its reconstructed approximation $u_{\varepsilon,1}$. We consider two ways to measure this difference:

- Our first measure of error is the difference between $u_\varepsilon(T,x)$ and $u_{\varepsilon,1}(T,x)$, at $T = 0.2$, in the relative $L^2(\Omega)$ norm, that is

$$\frac{\|u_\varepsilon(T,\cdot) - u_{\varepsilon,1}(T,\cdot)\|_{L^2(\Omega)}}{\|u_\varepsilon(T,\cdot)\|_{L^2(\Omega)}}. \tag{11}$$

  We plot on Figure 5 the difference $|u_\varepsilon(T,x) - u_{\varepsilon,1}(T,x)|$ at the time $T = 0.2$, for the two values of ε that we have considered.

- Second, we can consider an average (in space and time) error by monitoring the quantity

$$\frac{\|u_\varepsilon - u_{\varepsilon,1}\|_{L^2([0,T]\times\Omega)}}{\|u_\varepsilon\|_{L^2([0,T]\times\Omega)}}, \tag{12}$$

  where the final time of the interval $[0,T]$ is $T = 0.2$ (in practice, the $L^2(0,T)$ norm has been computed using one time step out of every 10 time steps).

The theoretical work [6] proves a convergence of $u_\varepsilon - u_{\varepsilon,1}$ to zero only in terms of the quantity (12), without providing any rate of convergence with respect to ε. The numerical results are shown in Table 1. For both criterias, we observe that the difference between u_ε and $u_{\varepsilon,1}$ becomes smaller when ε decreases, and that this convergence seems to be linear with respect to ε (dividing ε by 5 leads to the error being divided by 5). We also note that, to reach a relative error (12) of 10%, we need to take ε as small as $\varepsilon = 0.01$ (which corresponds to having 100 periods in each direction of the computational domain).

ε	Relative error (11)	Relative error (12)
0.05	1.21	0.504
0.01	0.181	0.100

Table 1 – Comparison between u_ε and $u_{\varepsilon,1}$ according to various criteria.

Table 1 thus shows that $u_{\varepsilon,1}$ is an accurate approximation of u_ε, provided ε is small enough. We now discuss computational costs. As pointed out above, we have chosen to use the same discretization parameters for the oscillatory and the homogenized problems, in order to not introduce any coarse discretization error. In practice, these discretization parameters can be chosen independently for both problems:

- for the oscillatory problem, we must take a mesh size h much smaller than ε, in order to capture the oscillations of the advection field; on the other hand, the time step can be chosen independently of ε.
- for the homogenized problem, the time step and the cell size can of course be chosen independently of ε, and should satisfy the CFL condition.

The computational cost of the direct method (discretizing u_ε) is thus much larger than the computational cost of the homogenized method (discretizing $u^\star$ and next evaluating $u_{\varepsilon,1}$) because of the much smaller mesh size h that it requires (on the other hand, the two problems can be discretized using the same time step). This discrepancy in terms of computational cost becomes larger when ε becomes smaller.

Given the above arguments, our temporary conclusion (which is of course yet to be confirmed, by considering for instance smaller values of ε) is that the homogenized method yields an approximation of the exact solution of the same accuracy as the direct method for a much smaller computational cost.

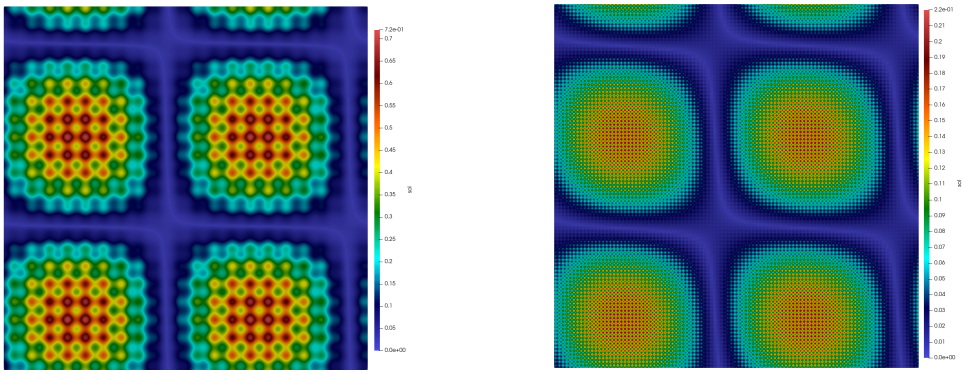

Figure 5 – Difference $|u_\varepsilon(T,x) - u_{\varepsilon,1}(T,x)|$ at time $T = 0.2$, for different values of ε (left: $\varepsilon = 0.05$; right: $\varepsilon = 0.01$).

2.3 Perspectives

We have just started to investigate multiscale hyperbolic problems. Until now, we have put in action the results of homogenization theory on a simple, linear case. There are several steps ahead of us, the first one being to

(i) extend our current numerical approach to the nonlinear setting, a setting which is actually relevant from the application viewpoint and which is theoretically covered in [6].

A long term agenda is to build a genuine multiscale approach for hyperbolic problems. We indeed underline that homogenization theory typically requires some geometric assumptions on the oscillatory functions of the equation under study. In the case of (1), it for instance requires the function $y \mapsto F(y,v)$ to be periodic. Such assumptions may be somewhat idealized with respect to practice (this is the case for the periodic assumption), or lead to very expensive computations (this is typically the case of a random stationary assumption). To address this issue in the context of elliptic and parabolic equations, several multiscale numerical methods have been proposed in the literature, based on finite element methods. We have significantly contributed to one of them, the Multiscale Finite Element Method (MsFEM). On this topic, our long-term objective is to

(ii) design a genuine multiscale approach that directly attacks the hyperbolic oscillatory equation, using homogenization theory as an intuitive guideline. Since Finite Volume techniques are often the method of choice for single-scale hyperbolic equations, and in particular conservation laws, it is natural to ask the

question of developing a multiscale finite volume method, that in spirit mimicks MsFEM, and plays for hyperbolic equations the role that MsFEM plays for diffusive equations. To the best of our knowledge, there exists only a few attempts in the literature to construct dedicated techniques for computing the solution to multiscale hyperbolic equations. We refer in particular to [11] and [9, Section 2.5.1], which both use *variants* of MsFEM. However, no such technique seems to be a genuine finite volume approach. The question we raise is actually already interesting and challenging in the linear setting.

This ambitious research program will not be completed within the current postdoctoral fellowship of Amandine Boucart. As suggested in our 2023 white paper [EOARD-WP], we hope to proceed with it in the context of a renewed funding.

3 Non-intrusive implementation of Multiscale Finite Element Methods

[Work expanded in [BLBLL23a, BLBLL23b, B-PhD]].

In this section, we explain how Multiscale Finite Element methods (MsFEM), which, we recall, are finite element type approaches dedicated to multiscale problems, can be implemented in a non-intrusive manner. We expect such non-intrusive implementations to eventually facilitate the dissemination of MsFEM methods within industrial codes or non academic environments. This is a topic that we have already very briefly mentioned in our 2021 report [EOARD-2021, Section 2.2.3], in a different context, and that we describe here in more details. This work has been completed within the PhD of Rutger Biezemans (see [B-PhD]), funded by a fellowship of the Paris Region. As already mentioned in the Executive Summary, this work, although not supported by EOARD, is part of the global research effort of the team and is closely related to the research performed in the context of the present contract.

Let us consider the highly oscillatory diffusion problem

$$-\operatorname{div}\left(A^\varepsilon \nabla u^\varepsilon\right) = f \ \text{ in } \Omega, \qquad u^\varepsilon = 0 \ \text{ on } \partial\Omega, \tag{13}$$

in a bounded domain $\Omega \subset \mathbb{R}^d$, where the diffusion coefficient A^ε is assumed to oscillate on a small length scale of typical size ε (the extension of our approach to other equations is discussed in Section 3.3 below). We seek a numerical approximation of (13) by applying a Galerkin approach. It is well-known that standard finite element methods

yield an approximation of poor accuracy, unless a prohibitively expensive fine mesh is employed. Dedicated multiscale approaches have thus been introduced, which provide a reasonably accurate approximation of (13) for a limited computational cost. In the sequel, we focus on one such method, the Multiscale Finite Element Method (MsFEM), that we have already considered in several of our previous reports, see e.g. [EOARD-2021] (we refer to [9, 13] for a comprehensive exposition). We recall that the MsFEM method is a finite element type method, which consists of two steps:

- an "offline" phase, where highly oscillatory, problem-dependent basis functions are numerically computed as solutions to local problems;
- an "online" phase, where a Galerkin approximation of (13), performed in the finite-dimensional space generated by the basis functions computed in the offline phase, is solved.

Several MsFEM variants exist, depending on the specific definition of the basis functions. But they are all definitely intrusive. They indeed require to change the finite element basis set and adjust it to the problem at hand. Our aim here is to explain how these approaches can be adapted so that they become as little intrusive as possible, thereby allowing to use only a *legacy*, single-scale software (based on standard finite elements) to recover an accurate approximation of (13).

In Section 3.1, we consider the example of the diffusion problem (13). We then introduce the simplest MsFEM approach (namely the so-called linear MsFEM) in a Galerkin setting, and present its non-intrusive variant. Some illustrative numerical results are provided in Section 3.2, to numerically quantify the additional error introduced by the non-intrusive implementation of the method. It is well-known that the linear MsFEM variant considered in Section 3.1 is outperformed by several MsFEM variants. For pedagogical purposes, we have deliberately chosen to present our ideas on this simple variant and to collect in Section 3.3 some concluding remarks on the many possible extensions of our methodology to design non-intrusive implementations of existing approaches.

3.1 Non-intrusive implementation of MsFEM: a simple case

We seek a numerical approximation of (13) by applying an MsFEM type Galerkin approach. To this end, we introduce a coarse mesh $\mathcal{T}_H$ of Ω (made of triangles if $d = 2$, tetrahedra if $d = 3$) and denote by V_H the usual conformal $\mathbb{P}_1$ approximation

space on $\mathcal{T}_H$. We respectively denote by

$$a^\varepsilon(u,v) = \int_\Omega \nabla v \cdot A^\varepsilon \nabla u \qquad \text{and} \qquad F(v) = \int_\Omega fv \tag{14}$$

the bilinear and linear forms associated to the variational formulation of (13).

For any interior vertex x_i of the mesh $\mathcal{T}_H$, let $\phi_i^{\mathbb{P}_1} \in V_H$ be the associated piecewise affine basis function, and let $\phi_i^\varepsilon \in H_0^1(\Omega)$ be the associated multiscale basis function, which, we recall, is defined by

$$\forall K \in \mathcal{T}_H, \qquad -\operatorname{div}\left(A^\varepsilon \nabla \phi_i^\varepsilon\right) = 0 \ \text{ in } K \quad \text{and} \quad \phi_i^\varepsilon = \phi_i^{\mathbb{P}_1} \ \text{ on } \partial K. \tag{15}$$

The MsFEM approach consists in computing the approximation $u_H^\varepsilon \in V_H^\varepsilon$ defined by the problem

$$\forall v_H^\varepsilon \in V_H^\varepsilon, \qquad a^\varepsilon(u_H^\varepsilon, v_H^\varepsilon) = F(v_H^\varepsilon), \tag{16}$$

where the multiscale approximation space is defined as

$$V_H^\varepsilon = \operatorname{Span}\left\{\phi_i^\varepsilon,\ 1 \le i \le N_v\right\}.$$

Implementing this method in an industrial code is challenging. No analytic expressions for the basis functions ϕ_i^ε are available (and thus a fine mesh should be used to approximate them), the computation of the stiffness matrix contributions $\displaystyle\int_K \nabla \phi_j^\varepsilon \cdot A^\varepsilon \nabla \phi_i^\varepsilon$ should be performed by quadrature rules on the fine mesh because the integrands are highly oscillatory, one should have at hand the correspondence between element and vertex indices in the coarse mesh, the assembly of the global stiffness matrix should be *manually* performed, etc. To alleviate these obstacles, we are going to introduce a way of implementing MsFEM that capitalizes on an existing code for solving (13) by a $\mathbb{P}_1$ approximation on $\mathcal{T}_H$ in the case of slowly-varying diffusion coefficients.

Our starting point for reducing intrusiveness is the following key observation. On any $K \in \mathcal{T}_H$, by linearity of the definition (15) of ϕ_i^ε in terms of $\phi_i^{\mathbb{P}_1}$, and because the finite element space V_H consists of functions that are piecewise affine (that is to say, $\nabla \phi_i^{\mathbb{P}_1}$ is constant in each K), we have the expansion

$$\phi_i^\varepsilon(x)|_K = \phi_i^{\mathbb{P}_1}(x) + \sum_{\alpha=1}^{d} (\partial_\alpha \phi_i^{\mathbb{P}_1})|_K \ \chi_K^{\varepsilon,\alpha}(x), \tag{17}$$

for any basis function ϕ_i^ε of V_H^ε, where $\chi_K^{\varepsilon,\alpha} \in H_0^1(K)$ is the solution to the local problem

$$-\operatorname{div}\left(A^\varepsilon \nabla \chi_K^{\varepsilon,\alpha}\right) = \operatorname{div}\left(A^\varepsilon e_\alpha\right) \quad \text{in } K, \qquad \chi_K^{\varepsilon,\alpha} = 0 \quad \text{on } \partial K, \tag{18}$$

where e_α denotes the α-th canonical unit vector of $\mathbb{R}^d$. We next extend $\chi_K^{\varepsilon,\alpha}$ by 0 outside K, thereby obtaining a function $\chi_K^{\varepsilon,\alpha} \in H_0^1(\Omega)$. We deduce from (17) that

$$\phi_i^\varepsilon = \phi_i^{\mathbb{P}_1} + \sum_{K \in \mathcal{T}_H} \sum_{\alpha=1}^{d} (\partial_\alpha \phi_i^{\mathbb{P}_1})|_K \ \chi_K^{\varepsilon,\alpha} \qquad \text{on } \Omega. \tag{19}$$

We now consider the linear system associated to (16) and insert therein the expansion (19) for the multiscale basis functions. The solution to (16) reads $u_H^\varepsilon = \sum_{i=1}^{N_v} U_i^\varepsilon \, \phi_i^\varepsilon$, where $U^\varepsilon = \left(U_1^\varepsilon, \ldots, U_{N_v}^\varepsilon\right)^T$ is the solution to

$$\mathbb{A}^\varepsilon \, U^\varepsilon = \mathbb{F}^\varepsilon, \tag{20}$$

with

$$\forall 1 \le i,j \le N_v, \qquad \mathbb{A}_{j,i}^\varepsilon = a^\varepsilon\left(\phi_i^\varepsilon, \phi_j^\varepsilon\right), \qquad \mathbb{F}_j^\varepsilon = F\left(\phi_j^\varepsilon\right).$$

Using that $\nabla \phi_i^{\mathbb{P}_1}$ is piecewise constant, we write

$$\nabla \phi_i^\varepsilon = \sum_{K \in \mathcal{T}_H} \sum_{\alpha=1}^{d} (\partial_\alpha \phi_i^{\mathbb{P}_1})|_K \ \left(e_\alpha + \nabla \chi_K^{\varepsilon,\alpha}\right).$$

Inserting this relation in the definition of the matrix elements $\mathbb{A}_{j,i}^\varepsilon$, we obtain

$$\begin{aligned}
\mathbb{A}_{j,i}^\varepsilon &= \int_\Omega \nabla \phi_j^\varepsilon \cdot A^\varepsilon \nabla \phi_i^\varepsilon \\
&= \sum_{K \in \mathcal{T}_H} \sum_{\alpha,\beta=1}^{d} (\partial_\beta \phi_j^{\mathbb{P}_1})|_K \ \left(\int_K \left(e_\beta + \nabla \chi_K^{\varepsilon,\beta}\right) \cdot A^\varepsilon \left(e_\alpha + \nabla \chi_K^{\varepsilon,\alpha}\right) \right) \ (\partial_\alpha \phi_i^{\mathbb{P}_1})|_K \\
&= \sum_{K \in \mathcal{T}_H} |K| \sum_{\alpha,\beta=1}^{d} (\partial_\beta \phi_j^{\mathbb{P}_1})|_K \ \left.\overline{A}_{\beta,\alpha}\right|_K \ (\partial_\alpha \phi_i^{\mathbb{P}_1})|_K,
\end{aligned} \tag{21}$$

where the piecewise constant matrix-valued field $\overline{A} \in \mathbb{P}_0(\mathcal{T}_H, \mathbb{R}^{d\times d})$ is defined by

$$\left.\overline{A}_{\beta,\alpha}\right|_K = \frac{1}{|K|} \, a_K^\varepsilon\left(x^\alpha + \chi_K^{\varepsilon,\alpha}, x^\beta + \chi_K^{\varepsilon,\beta}\right) \tag{22}$$

for each $K \in \mathcal{T}_H$ and $1 \leq \alpha, \beta \leq d$, where $|K|$ denotes the area or volume of the mesh element K.

Motivated by (21), we introduce the coarse-scale problem

$$-\operatorname{div}\left(\overline{A}\,\nabla u\right) = f \ \text{ in } \Omega, \qquad u = 0 \ \text{ on } \partial\Omega, \tag{23}$$

and its $\mathbb{P}_1$ Galerkin discretization: find $u_H \in V_H$ such that

$$\forall v_H \in V_H, \qquad a^{\overline{A}}(u_H, v_H) = F(v_H), \tag{24}$$

where the linear form F is defined by (14) and the bilinear form $a^{\overline{A}}$ is defined by

$$\forall u, v \in H^1_0(\Omega), \quad a^{\overline{A}}(u,v) = \sum_{K\in\mathcal{T}_H} a_K^{\overline{A}}(u,v) \quad \text{with} \quad a_K^{\overline{A}}(u,v) = \int_K \nabla v \cdot \overline{A}\nabla u.$$

Problem (24) equivalently writes

$$\mathbb{A}^{\mathbb{P}_1} U^{\mathbb{P}_1} = \mathbb{F}^{\mathbb{P}_1}, \tag{25}$$

with

$$\forall 1 \leq i,j \leq N_v, \qquad \mathbb{A}^{\mathbb{P}_1}_{j,i} = a^{\overline{A}}\left(\phi_i^{\mathbb{P}_1}, \phi_j^{\mathbb{P}_1}\right), \qquad \mathbb{F}^{\mathbb{P}_1}_j = F\left(\phi_j^{\mathbb{P}_1}\right).$$

We then deduce from (21) that

$$\mathbb{A}^{\varepsilon}_{j,i} = \int_\Omega \nabla\phi_j^{\mathbb{P}_1} \cdot \overline{A}\nabla\phi_i^{\mathbb{P}_1} = \mathbb{A}^{\mathbb{P}_1}_{j,i}, \tag{26}$$

where we recall that the piecewise constant matrix $\overline{A}$ given by (22), and therefore the stiffness matrix $\mathbb{A}^{\mathbb{P}_1}$, depends on the fine-scale oscillations of A^ε.

The above calculations yield that the stiffness matrix $\mathbb{A}^\varepsilon$ in the MsFEM problem (20) is identical to the stiffness matrix $\mathbb{A}^{\mathbb{P}_1}$ in the $\mathbb{P}_1$ problem (25). We however note that the right-hand vector $\mathbb{F}^\varepsilon$ in (20) is in general different from the right-hand side vector $\mathbb{F}^{\mathbb{P}_1}$ in (25), since we integrate f against highly oscillatory basis functions in the former problem and against $\mathbb{P}_1$ basis functions in the latter. The solutions U^ε and $U^{\mathbb{P}_1}$ to (20) and (25), respectively, are thus a priori different.

The above observations suggest to use the identity (26) of the stiffness matrices to replace the MsFEM discrete problem (20) by the discrete problem (25) stemming from the $\mathbb{P}_1$ Galerkin approximation of the *single scale* problem (23), which itself may be easily implemented in legacy codes. The superiority of that implementation over the classical MsFEM implementation is that the global problem of the online phase

(including its right-hand side) can be completely constructed and solved using a pre-existing $\mathbb{P}_1$ PDE solver. The only requirements in the legacy code are the ability to provide piecewise constant diffusion coefficients to the solver (and the existence of a procedure which provides the value of the solution at any point in Ω, in order to eventually reconstruct the oscillatory solution u_H^ε). Note also that the fine-scale problem (18) is only indexed by the coarse mesh element K, in contrast to the fine-scale problem (15), which is indexed both by the coarse mesh element K and the vertex index i. In the latter case, one has to know, for each element K, the global number of the element vertices, a piece of information which may be difficult to access to in a legacy code. In the former case, this correspondence is not needed to compute $\overline{A}$, which is entirely defined element-wise.

To summarize, the above procedure to go from the MsFEM problem (16) to its non-intrusive implementation is based on the following steps:

1. we use the linearity of the problem and the fact that gradients of $\mathbb{P}_1$ basis functions are constant in each mesh element to establish the identity (17);

2. we can then recast the MsFEM stiffness matrix $\mathbb{A}^\varepsilon$ as the stiffness matrix $\mathbb{A}^{\mathbb{P}_1}$ of the $\mathbb{P}_1$ discretization of an appropriate problem;

3. we approximate the right-hand side $\mathbb{F}^\varepsilon$ of the MsFEM problem by a right-hand side $\mathbb{F}^{\mathbb{P}_1}$ which can be computed in a manner consistent with a $\mathbb{P}_1$ discretization;

4. we postprocess the $\mathbb{P}_1$ solution to obtain an approximation of the reference solution.

We expect the computational cost of the non-intrusive implementation to be smaller, since $\mathbb{F}^{\mathbb{P}_1}$ is cheaper to compute than $\mathbb{F}^\varepsilon$ (we do not need to use a quadrature rule on the fine mesh). On the other hand, the non-intrusive implementation may introduce additional numerical errors, that we now investigate.

3.2 Numerical results

We now present some illustrating numerical examples (we refer for other examples to [BLBLL23a, BLBLL23b]). We take $\Omega = (0,1)^2$, $f(x) = \sin(x_1)\,\sin(x_2)$ and

$$A^\varepsilon(x) = 1 + \left(1 + 100\cos^2(\pi x_1/\varepsilon)\sin^2(\pi x_2/\varepsilon)\right)\cos^2\left(\frac{x_1^2 + x_2^2}{\varepsilon}\right).$$

We deliberately consider here a non-periodic case. Recall indeed that the purpose of MsFEM approaches is to address general multiscale settings. In contrast to quantitative homogenization theory, their implementation does not rely on any geometric assumption on the microstructure, such as periodicity. For $\varepsilon = \pi/150 \approx 0.02$, we consider the reference solution $u_{\rm ref}$ (computed in practice on a fine mesh of size $h = 1/1024$), and, for various values of H (ranging from 1/4 to 1/256), the solution $u_H^{\varepsilon,G}$ to the Galerkin approximation (16) and the solution $u_H^{\varepsilon,{\rm ni}}$ to the non-intrusive implementation. In Table 2, we show the error $\left\|u_H^{\varepsilon,G} - u_{\rm ref}\right\|_{H^1(\Omega)}$ and the difference $\left\|u_H^{\varepsilon,G} - u_H^{\varepsilon,{\rm ni}}\right\|_{H^1(\Omega)}$. We observe that the difference $u_H^{\varepsilon,G} - u_H^{\varepsilon,{\rm ni}}$ is extremely small (here by a factor of at least 200) in comparison to the error $u_H^{\varepsilon,G} - u_{\rm ref}$. The intrusive and the non-intrusive MsFEMs thus share the same accuracy, and this numerical observation can be backed up by some theoretical arguments presented in [BLBLL23a].

Table 2 – Errors between $u_H^{\varepsilon,G}$, $u_H^{\varepsilon,{\rm ni}}$ and $u_{\rm ref}$ for several values of H.

H/ε	$\left\|u_H^{\varepsilon,G} - u_{\rm ref}\right\|_{H^1(\Omega)}$	$\left\|u_H^{\varepsilon,G} - u_H^{\varepsilon,{\rm ni}}\right\|_{H^1(\Omega)}$
11.94	8.69×10^{-3}	2.32×10^{-5}
5.97	7.11×10^{-3}	3.22×10^{-5}
2.98	8.81×10^{-3}	2.59×10^{-5}
1.49	1.12×10^{-2}	2.51×10^{-5}
0.75	1.30×10^{-2}	1.53×10^{-5}
0.37	1.07×10^{-2}	9.85×10^{-6}
0.19	7.55×10^{-3}	4.00×10^{-6}

3.3 Concluding remarks on possible extensions

Despite the fact that it significantly improves upon the classical FEM approach, the MsFEM approach using the basis functions ϕ_i^ε defined by (15) suffers from a well-known shortcoming, due to the fact that *affine* boundary conditions are imposed for ϕ_i^ε. The method cannot yield an accurate approximation of the reference solution u^ε near the edges of the coarse mesh elements, since the exact solution oscillates along the edges while the numerical approximation does not. To overcome this drawback, several alternative definitions of the multiscale basis functions have been proposed,

leading to different MsFEM variants, including the oversampling variant, introduced in [10] and nowadays considered to be a reference MsFEM variant. We have shown in [BLBLL23b] how the non-intrusive implementation procedure presented here can be extended to that case.

To outline the versality of the above procedure leading to a non-intrusive implementation, we eventually make a few remarks on the advection-diffusion problem

$$-\operatorname{div}(A^\varepsilon \nabla u^\varepsilon) + b \cdot \nabla u^\varepsilon = f \ \text{ in } \Omega, \qquad u^\varepsilon = 0 \ \text{ on } \partial\Omega.$$

The MsFEM basis functions may be defined by (15) or by a similar equation including the advection term (see e.g. [16, B-PhD]). Oversampling may also be used. In all cases, for the same reasons as above, an identity of the type (17) holds, which allows to express the stiffness matrix of the approach as the stiffness matrix obtained using a standard $\mathbb{P}_1$ finite element approximation of a single-scale problem containing diffusion and advection terms, with appropriate definitions of an effective diffusion matrix $\overline{A}$ and an effective advection field $\overline{b}$ that are both piecewise constant.

4 Coarse approximations for Schrödinger problems with highly oscillatory potentials

We wish to test on the specific setting of the Schrödinger equation whether and how we may reconstruct (part of) the oscillatory coefficient entering the equation from the data, i.e. from the solutions of the equation for several right-hand sides. To this end, we have to first lay some groundwork, which consists in revisiting an approach we introduced earlier in [14, 15] in the context of the diffusion equation, in order to adjust and adapt it to the specificities of the Schrödinger equation. These elements, already presented in [EOARD-2022], are briefly summarized in Sections 4.1 and 4.2. In Section 4.3, we present some detailed numerical results concerning the approximation of the effective (homogenized) coefficients and of the solution to the oscillatory equation, in a multi-dimensional setting (in contrast to our previous report [EOARD-2022], where these numerical tests were performed in the one-dimensional setting). We then collect in Section 4.4 some conclusions and perspectives. The works we describe in this section have been completed within the PhD of Simon Ruget, who joined the team in Fall 2022 (see [R-PhD]), and the fellowship of whom is funded by Inria. As already mentioned in the Executive Summary, this work, although not supported by EOARD, is part of the global research effort of the team and is closely related to the research performed in the context of the present contract.

4.1 Context

We consider the following problem, which is the so-called *Schrödinger equation with rapidly oscillating potential*:

$$-\Delta u_\varepsilon + \frac{1}{\varepsilon} W^\varepsilon \, u_\varepsilon = f \ \text{ in } \Omega, \qquad u_\varepsilon = 0 \ \text{ on } \partial\Omega, \tag{27}$$

where Ω is a bounded domain in $\mathbb{R}^d$ and W^ε is a potential function that oscillates at the small scale ε. Solving (27) is of course numerically challenging, since its solution u_ε oscillates at a small scale.

Before presenting our approach, it is useful to recall the following homogenization result, in the periodic setting. We assume that $W^\varepsilon(x) = W(x/\varepsilon)$, where W is a fixed Y-periodic function and Y is the unit cell $Y = (0,1)^d$, the mean of which vanishes:

$$\int_Y W = 0. \tag{28}$$

By virtue of (28), we can find a Y-periodic function χ, which we call hereafter the corrector, such that

$$\Delta \chi = W. \tag{29}$$

We next define

$$W_\star = \int_Y W \, \chi = -\int_Y |\nabla \chi|^2.$$

In order to proceed with the homogenization of (27), we also assume that $\lambda_1 + W_\star > 0$, where λ_1 is the smallest eigenvalue of the Laplacian operator in Ω supplied with homogeneous Dirichlet boundary conditions.

Let us now introduce the homogenized equation

$$-\Delta u_\star + W_\star \, u_\star = f \ \text{ in } \Omega, \qquad u_\star = 0 \ \text{ on } \partial\Omega. \tag{30}$$

It is well-known (see e.g. [4, Theorem 12.1]) that, under the above assumptions, the oscillatory problem (27) (resp. the homogenized problem (30)) admits a unique solution $u_\varepsilon \in H^1_0(\Omega)$ for any ε sufficiently small (resp. a unique solution $u_\star \in H^1_0(\Omega)$) and that, when ε goes to 0, u_ε converges weakly in $H^1(\Omega)$ to $u_\star$.

Furthermore, using the corrector χ, and as is classical in homogenization, it is possible to provide an approximation of u_ε in the *strong norm*. We indeed have (see e.g. [4, Theorem 12.3])

$$\lim_{\varepsilon \to 0} \| u_\varepsilon - (u_\star + \varepsilon \, \chi^\varepsilon \, u_\star) \|_{H^1(\Omega)} = 0, \tag{31}$$

where χ^ε is defined by $\chi^\varepsilon(x) = \chi(x/\varepsilon)$ for any $x \in \Omega$ and where the corrector χ is defined by (29).

We now return to the oscillatory equation (27) and do not make any periodicity (or any other geometric) assumption on W^ε. The question we investigate is to find the best non-oscillating potential $\overline{W}$ (think e.g. of a constant potential) that is consistent, in a sense to be made precise, with the behavior of the highly oscillatory problem (27). Put differently, we wish to approximate the solution u_ε to (27) by the solution $\overline{u}$ to a similar problem with a *constant* potential $\overline{W}$, which reads

$$-\Delta \overline{u} + \overline{W}\, \overline{u} = f \ \text{ in } \Omega, \qquad \overline{u} = 0 \ \text{ on } \partial\Omega. \tag{32}$$

Note of course the resemblance between (30) and (32).

The motivation for this approach is to find a pathway alternative to standard homogenization techniques when the latter are difficult to use in practice. Indeed, homogenization theory (e.g. as recalled above in the periodic setting) requires a complete knowledge of the oscillatory potential W^ε (e.g. to compute the corrector). In many practical cases, this coefficient is only partially known, or one only has access to the solution of (27) for some right-hand sides f.

When ε is asymptotically small, $\overline{W}$ should then be a fair approximation (for all practical purposes) of the homogenized potential $W_\star$. We introduce below an optimization formulation (see (33)–(35)) and show that this is indeed the case: when $\varepsilon \to 0$, the best constant potential converges to $W_\star$. The approach can thus be employed to approximate $W_\star$. In addition, when ε is not small, our strategy still provides an effective model, where the coefficients are the best possible in the optimization space in which we work.

4.2 A quadratic optimization formulation

We now recall our optimization procedure, as already introduced in our previous report [EOARD-2022]. For any constant potential $\overline{W} \in \mathbb{R}$, consider the problem with constant coefficients (32). For any fixed ε, we wish to define a constant $\overline{W}_\varepsilon \in \mathbb{R}$ such that the solution $\overline{u}_\varepsilon$ to (32) with $\overline{W} = \overline{W}_\varepsilon$ best approximates the solution u_ε to (27).

Inspired by [15], we could define $\overline{W}_\varepsilon$ as a minimizer of

$$\inf_{\overline{W}\in\mathbb{R}} \sup_{f\in L^2(\Omega),\ \|f\|_{L^2(\Omega)}=1} J_\varepsilon(\overline{W}, f), \tag{33}$$

with

$$J_\varepsilon(\overline{W}, f) = \|u_\varepsilon(f) - \overline{u}(f)\|^2_{L^2(\Omega)} \tag{34}$$

where we have emphasized the dependency upon the right-hand side f of the solutions to (27) and (32). In practice, solving the problem (33)–(34) is difficult, because it is *nonconvex*. Following [14], we prefer to actually define the constant $\overline{W}_\varepsilon$ as a minimizer of (33), where the cost function is now defined by

$$J_\varepsilon(\overline{W}, f) = \Big\| (-\Delta)^{-1} \Big(-\Delta u_\varepsilon(f) + \overline{W}\, u_\varepsilon(f) - f \Big) \Big\|^2_{L^2(\Omega)}, \tag{35}$$

where the operator $(-\Delta)^{-1}$ is defined by

$$w = (-\Delta)^{-1} g \quad \text{when} \quad -\Delta w = g \ \text{ in } \Omega \ \text{ and } \ w = 0 \ \text{ on } \partial\Omega.$$

Note that the cost function (35) is related to (34) through the application, inside the L^2 norm, of the operator $v \mapsto (-\Delta)^{-1}\Big(-\Delta v + \overline{W}\, v \Big)$.

Let us now briefly recall the practical procedure to solve (33)–(35). We emphasize that (35) is quadratic with respect to f and $\overline{W}$, in contrast to (34). The problem (33)–(35) thus has the advantage of being *convex*. This is of paramount importance for the efficiency of the numerical approach.

The supremum over $f \in L^2(\Omega)$ in (33) is approximated by a supremum over a finite-dimensional space. More precisely, problem (33) is approximated by

$$\inf_{\overline{W}\in\mathbb{R}} \sup_{f\in V_P,\ \|f\|_{L^2(\Omega)}=1} J_\varepsilon(\overline{W}, f), \tag{36}$$

where V_P is the finite dimensional space generated by the first P eigenfunctions of the Laplacian operator on Ω, that is

$$V_P = \mathrm{Span}\left\{ \widetilde{f}_p,\ 1 \le p \le P \right\}, \tag{37}$$

where $-\Delta \widetilde{f}_p = \lambda_p\, \widetilde{f}_p$ on Ω with $\widetilde{f}_p = 0$ on $\partial\Omega$.

The minimization problem over $\overline{W}$ that is involved in (36), namely

$$\inf_{\overline{W}\in\mathbb{R}} J_\varepsilon(\overline{W}, f), \tag{38}$$

can be easily solved. For any fixed $f \in L^2(\Omega)$, we indeed observe, using the linearity of the operators, that the quantity $J_\varepsilon(\overline{W}, f)$ is a polynomial function of degree 2 with respect to $\overline{W}$. The solution of the inf problem (38) is hence analytically known.

The maximization problem over f that is involved in (36), namely

$$I_P = \sup_{f\in V_P,\ \|f\|_{L^2(\Omega)}=1} J_\varepsilon(\overline{W}, f), \tag{39}$$

is also easy to solve, once V_P has been chosen as (37). For a fixed $\overline{W}$, it indeed amounts to computing the largest eigenvalue of a symmetric positive definite matrix $\mathbb{A}(\overline{W})$, of size $P \times P$, and the associated eigenvector. The maximum I_P in (39) is equal to the largest eigenvalue.

To solve the inf sup problem (36) in practice, we alternate between the maximization problem (39) and the minimization problem (38).

4.3 Numerical results: effective potential and approximation of the solution

Theoretical results concerning our approach (33)–(35) have been presented in our previous report [EOARD-2022]. Likewise, some illustrating numerical results in the one-dimensional setting have been provided there. As pointed out in the Executive Summary, we now present a complete numerical investigation of the approach in a *multi-dimensional setting*.

In this section, we investigate the accuracy (with respect to the homogenized potential) of the best constant potential $\overline{W}_\varepsilon^{\rm opt}$ provided by our approach. We also describe how to use $\overline{W}_\varepsilon^{\rm opt}$ to approximate the solution u_ε to the oscillatory equation. In short, the numerical experiments reported below show that our approach, in the setting considered here, provides an accurate approximation of $W_\star$ and of u_ε, as soon as ε is sufficiently small (here $\varepsilon \leq 0.1 = |\Omega|/10$), and that it only requires a few iterations to solve (33)–(35). In a multi-query context (where one considers (27) for many right-hand sides), it is thus much less expensive than a direct approach discretizing (27).

We now detail our setting. We work with $\Omega = (0,1)^2$ and the potential

$$W(x,y) = \pi^2\sqrt{8}\,(\sin(2\pi x) + \sin(2\pi y))\,.$$

The prefactor in this potential has been specifically chosen such that the homogenized potential $W_\star$ is comparable to the first eigenvalue $\lambda_1 = 2\pi^2$ of the Laplacian operator on Ω. We actually have $-W_\star = |W_\star| = \lambda_1/2$. In the homogenized equation (30), the two terms of the left-hand side thus have roughly the same magnitude, and the test case thus does not correspond to a small perturbation of the Laplacian operator, a case which is too simple.

In practice, here, the oscillatory equation (27) and the effective equation (32) are solved using a finite element method, both on the same fine mesh (in order to not introduce any coarse discretization error). The size of the mesh elements is sufficiently small to ensure that u_ε (and a fortiori $\overline{u}$) are accurately computed. For any ε, we start

the optimisation procedure from the initial guess $\overline{W} = 0$ (which corresponds to the average of W).

4.3.1 Computation of the effective potential

We first observe that our alternate direction algorithm to solve (36) converges in a few iterations, as shown on Figure 6a. When ε is sufficiently small, the relative error between the homogenized potential $W_\star$ and the optimal effective potential $\overline{W}_\varepsilon^{\rm opt}$ provided by our approach is small (see Figure 6b). Of course, when ε is not small, $\overline{W}_\varepsilon^{\rm opt}$ has no reason to be close to $W_\star$.

More precisely, as soon as the space V_P contains the first eigenelement of the Laplacian operator, i.e. as soon as V_P is given by (37) for some P, the results are extremely good and actually independent of P. For any value $\varepsilon \leq 0.1$, the relative error between $\overline{W}_\varepsilon^{\rm opt}$ and $W_\star$ is smaller than 1%. In addition, the convergence of $\overline{W}_\varepsilon^{\rm opt}$ to $W_\star$ seems to occur at a quadratic rate with respect to ε, in the sense that $\left|\overline{W}_\varepsilon^{\rm opt} - W_\star\right| \propto \varepsilon^2$.

If V_P does not include the first eigenelement of the Laplacian operator (this corresponds to the green curve on Figure 6b, where $V_P = \mathrm{Span}\left\{\widetilde{f}_p,\ 2 \leq p \leq 10\right\}$), we observe that the optimum value $\overline{W}_\varepsilon^{\rm opt}$ still converges to $W_\star$ when $\varepsilon \to 0$, again at a quadratic rate, but with a larger prefactor. Nevertheless, the error remains small: for any value $\varepsilon \leq 0.1$, the relative error is already as small as 5%.

All these results confirm our claim that our approach indeed allows to obtain a very accurate approximation of $W_\star$.

4.3.2 Approximation of the solution in L^2 norm

We now investigate the accuracy of our approximation, in terms of recovering the solution to the problem. We are thus going to compare, for various right-hand sides f, the solution $u_\varepsilon(f)$ to the oscillatory equation (27) and the solution $\overline{u}(f)$ to the effective equation (32) using the optimal effective potential $\overline{W}_\varepsilon^{\rm opt}$. For this comparison, we set $P = 1$ in the choice of the learning space V_P defined by (37). Stated otherwise, the optimal effective potential $\overline{W}_\varepsilon^{\rm opt}$ is computed using $V_P = \mathrm{Span}\left\{\widetilde{f}_1\right\}$. We have seen on Figure 6b that this choice leads to a converging approximation of $W_\star$ when $\varepsilon \to 0$.

The accuracy of $\overline{u}(f)$ is here quantified by the criterion

$$\sup_{f \in V_Q} \frac{\|\overline{u}(f) - u_\varepsilon(f)\|_{L^2(\Omega)}}{\|u_\varepsilon(f)\|_{L^2(\Omega)}}, \tag{40}$$

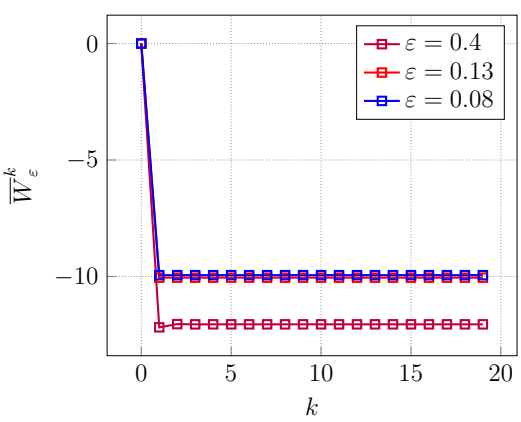

(a) Value of $\overline{W}_\varepsilon^k$ along the iterations k (for three different values of ε).

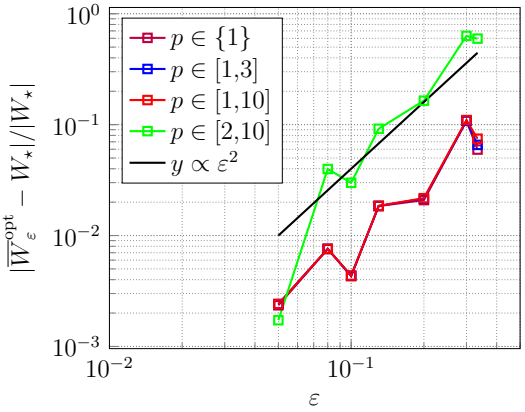

(b) Relative error between $\overline{W}_\varepsilon^{\mathrm{opt}}$ and $W_\star$, for various choices of V_P (the results for $p \in \{1\}$, $p \in [1,3]$ and $p \in [1,10]$ lie on top of each other).

Figure 6 – Performance of our approach in terms of effective potential.

where V_Q is the space of dimension Q defined by (37). On Figure 7a, we consider the case $Q = P$ (here $Q = 1$), which means that we plot the quantity that we have minimized in order to define $\overline{W}_\varepsilon^{\mathrm{opt}}$. On Figure 7b, we next consider the choice $Q \gg P$ (here $Q = 10$), which means that we test the quality of our approximation $\overline{u}(f)$ for right-hand sides f that we did not consider when searching for the optimal effective potential. We again observe accurate results as soon as $\varepsilon \leq 0.1$, with the relative error (40) (computed for $Q = 10$) being smaller than 7%. When ε is too large, there is no reason for the approximation (32) (using a *constant* effective potential) to be accurate.

4.3.3 Approximation of the solution in H^1 norm

Besides $W_\star$ (which is well approximated by $\overline{W}_\varepsilon^{\mathrm{opt}}$) or u_ε (which is well approximated by $\overline{u}$ in the L^2 norm, a function which is easy to compute once $\overline{W}_\varepsilon^{\mathrm{opt}}$ has been identified), another quantity of interest is ∇u_ε. In the same spirit, we recall (see (31)) that homogenization not only provides an approximation (in the L^2 norm) of u_ε, but also of ∇u_ε. To compare in a fair manner homogenization and our approach, we thus need to find a way, once an optimal $\overline{W}_\varepsilon^{\mathrm{opt}}$ has been determined, to recover an approximation of ∇u_ε (or equivalently of $\nabla \chi^\varepsilon$). For the diffusion equation, we have introduced several strategies to do so in [14, 15], and we adapt them here to the current setting.

In view of (31), we know that the function $u_{\varepsilon,1}$ defined by $u_{\varepsilon,1}(x) = u_\star(x)(1 +$

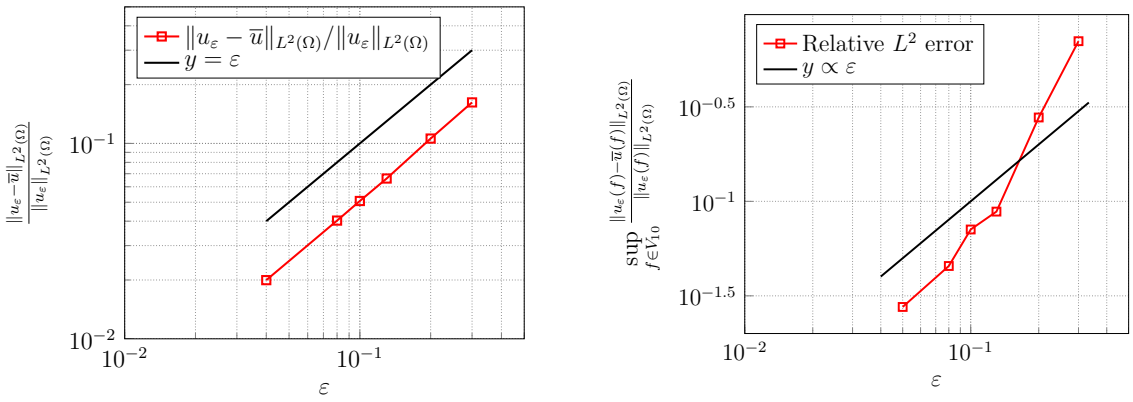

(a) The case $Q = P = 1$.

(b) The case $Q = 10$, $P = 1$.

Figure 7 – Relative error (40) between u_ε and $\overline{u}$.

$\varepsilon\chi(x/\varepsilon)$) is a good H^1 approximation of the function u_ε. We hence have

$$\nabla u_\varepsilon(x) \approx \nabla u_\star(x) + u_\star(x)\, \nabla\chi\left(\frac{x}{\varepsilon}\right).$$

Inspired by this relation, we define the vector-valued function $\overline{C}_\varepsilon$, which aims at approximating $\nabla\chi(\cdot/\varepsilon)$, as the minimizer of

$$\inf_{C \in \mathbb{P}_h^0} \sup_{f \in L^2(\Omega),\ \|f\|_{L^2(\Omega)}=1} \left\| \nabla u_\varepsilon(f) - \nabla\overline{u}\left(\overline{W}_\varepsilon^{\rm opt}, f\right) - \overline{u}\left(\overline{W}_\varepsilon^{\rm opt}, f\right) C \right\|_{L^2(\Omega)}^2. \tag{41}$$

In the above relation, $\overline{W}_\varepsilon^{\rm opt}$ is the optimal effective potential, identified in the first stage of the approach. We have seen that $\overline{W}_\varepsilon^{\rm opt} \approx W_\star$, and we therefore consider $\overline{u}(\overline{W}_\varepsilon^{\rm opt}, f)$ as an accurate approximation of $u_\star(f)$.

In a similar manner as for the identification of the best effective potential, we approximate the supremum over $f \in L^2(\Omega)$ in (41) by a supremum over the finite-dimensional space V_P defined by (37).

In (41), the vector-valued function C is searched among the piecewise constant functions (on a fine mesh $\mathcal{T}_h$ of size $h \ll \varepsilon$). Since the values of C are thus independent from one element to the next, the problem can be recast as a collection of problems on each element κ of the fine mesh:

$$\inf_{C_\kappa \in \mathbb{R}^d} \sup_{f \in V_P,\ \|f\|_{L^2(\Omega)}=1} \left\| \nabla u_\varepsilon(f) - \nabla\overline{u}\left(\overline{W}_\varepsilon^{\rm opt}, f\right) - \overline{u}\left(\overline{W}_\varepsilon^{\rm opt}, f\right) C_\kappa \right\|_{L^2(\kappa)}^2, \tag{42}$$

each of these problems being inexpensive to solve since the functional to minimize is quadratic with respect to C_κ. For technical reasons related to the discretization of $\overline{u}$, we do not perform this computation for the elements too close to the boundary $\partial\Omega$, but only for the elements contained in a domain $\Omega_{\rm int}$ isolated from the boundary of Ω. Denoting $C_\kappa^{{\rm opt},\varepsilon}$ the minimizer of (42), we eventually define $\overline{C}_\varepsilon$ on $\Omega_{\rm int}$ by $\overline{C}_\varepsilon(x) = \displaystyle\sum_{\kappa\in\mathcal{T}_h,\ \kappa\subset\Omega_{\rm int}} C_\kappa^{{\rm opt},\varepsilon}\, 1_\kappa(x)$.

We now investigate the accuracy of our approximation, and consider two criteria to quantify the error. In both cases, we set $P = 1$ in the choice of the learning space V_P defined by (37). Stated otherwise, the optimal effective potential $\overline{W}_\varepsilon^{\rm opt}$ and the optimal $\overline{C}_\varepsilon$ are computed using $V_P = {\rm Span}\left\{\widetilde{f}_1\right\}$. We can first monitor how well $\overline{C}_\varepsilon$ approximates $\nabla\chi(\cdot/\varepsilon)$ by computing the relative error

$$\frac{\|\overline{C}_\varepsilon - \nabla\chi(\cdot/\varepsilon)\|_{L^2(\Omega_{\rm int})}}{\|\nabla\chi(\cdot/\varepsilon)\|_{L^2(\Omega_{\rm int})}}. \tag{43}$$

Results are shown on Figure 8b and indeed demonstrate that $\overline{C}_\varepsilon$ is an accurate approximation of $\nabla\chi(\cdot/\varepsilon)$.

We can also compare, for various right-hand sides f, the gradient of the solution to the oscillatory equation (27) with its approximation provided by our approach, namely

$$\sup_{f\in V_Q} \frac{\left\|\nabla u_\varepsilon(f) - \nabla\overline{u}\left(\overline{W}_\varepsilon^{\rm opt}, f\right) - \overline{u}\left(\overline{W}_\varepsilon^{\rm opt}, f\right)\,\overline{C}_\varepsilon\right\|_{L^2(\Omega_{\rm int})}}{\|\nabla u_\varepsilon(f)\|_{L^2(\Omega_{\rm int})}}, \tag{44}$$

where V_Q is the space of dimension Q defined by (37). Results are shown on Figure 8a with the choice $Q \gg P$ (here $Q = 10$), which means that we test the quality of our approximation for right-hand sides that we did not consider when searching for the optimal effective model. We again observe accurate results as soon as $\varepsilon \leq 0.1$, with the relative error (44) (computed for $Q = 10$) being smaller than 7%.

4.4 Conclusions and perspectives

We collect here conclusions and directions of future research on this topic.

As pointed out above, the numerical tests of Section 4.3 demonstrate the efficiency of our approach to compute effective coefficients for the problem on the large scales and to provide an approximation (in various norms) of the oscillatory solution.

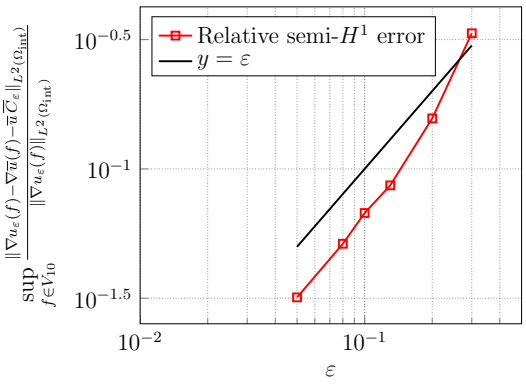

(a) Approximation of ∇u_ε by $\nabla \overline{u} + \overline{u}\,\overline{C}_\varepsilon$. The test space V_Q (with $Q = 10$) is much larger than the learning space V_P (with $P = 1$).

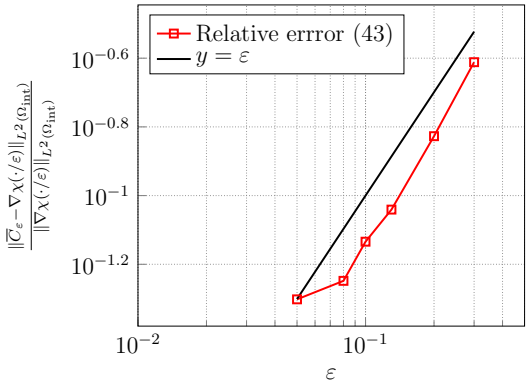

(b) Approximation of $\nabla\chi(\cdot/\varepsilon)$ by $\overline{C}_\varepsilon$.

Figure 8 – Performance of our approach to recover the solution in H^1 norm (in the two figures, both $\overline{W}_\varepsilon^{\rm opt}$ and $\overline{C}_\varepsilon$ have been computed using V_P with $P = 1$).

The main direction of research that we now wish to investigate is that of the robustness of our approach with respect to the available data. Note indeed that we have worked until now under the assumption that we have at our disposal the *complete* knowledge of u_ε for some right-hand sides. In practice, the data may be blurred or incomplete, because of

- noise introduced in the experimental measurement of u_ε.
- the fact that the experimental apparatus cannot measure u_ε at the fine scales, but only at the large scales. We can e.g. think of a situation where we only have access to averages of u_ε on the domain occupied by the experimental sensor, which is small compared to Ω but much larger than ε. We thus have to understand how to adapt the formulations (33)–(34) or (33)–(35) to the case where the only available data is of the form $\displaystyle\int_{B_H(x)} u_\varepsilon$, where $B_H(x)$ is a domain of size H satisfying $\varepsilon \ll H \ll \text{diam}\,\Omega$. Obviously, the high frequency oscillations of u_ε are lost, and the only quantity we may hope to identify is the effective coefficient of the system (in the present case, the effective potential $W_\star$).
- in mechanical experiments, the available data may not be the average of the displacement u_ε, but the average of the deformation tensor $e(u_\varepsilon) = (\nabla u_\varepsilon + (\nabla u_\varepsilon)^T)/2$. Actually, it may even be the case that the average of only some

components of $e(u_\varepsilon)$ (those aligned with the experimental sensor) is available.

- etc.

We can also think of situations where we do not have access to (a coarse approximation of) the field u_ε, but only to averages of u_ε (or of related quantities) on the boundary of Ω. Think e.g., in a mechanical context, of having access to the average displacement / average force acting on the boundary of the specimen. This typically leads to the knowledge of the energy contained in the system, which reads, in the current Schrödinger context, as $E_\varepsilon(f) = \displaystyle\int_\Omega |\nabla u_\varepsilon|^2 + \frac{1}{\varepsilon}\int_\Omega W^\varepsilon\, u_\varepsilon^2$, where u_ε is the solution to the oscillatory problem (27) for the right-hand side f. Introducing the effective energy $E(\overline{W}, f) = \displaystyle\int_\Omega |\nabla \overline{u}|^2 + \int_\Omega \overline{W}\,\overline{u}^2$, where $\overline{u}$ is the solution to the effective problem (32) for the right-hand side f and the effective potential $\overline{W}$, a possible formulation is to define the best effective potential as the minimizer of

$$\inf_{\overline{W}\in\mathbb{R}} \sup_{f\in L^2(\Omega),\ \|f\|_{L^2(\Omega)}=1} \left| E(\overline{W}, f) - E_\varepsilon(f) \right|. \tag{45}$$

It is an interesting question to understand whether this formulation is well-posed, whether it leads, in a periodic setting, to some $\overline{W}_\varepsilon^{\rm opt}$ which converges, when $\varepsilon \to 0$, to the homogenized potential $W_\star$, and how it can solved efficiently.

We make the following additional remark. In many cases, we have an a priori empirical knowledge of the effective coefficients. In the Schrödinger setting, this means that the problem is not to search for the best $\overline{W}$ in the *whole* set $\mathbb{R}$, but rather to search for the best $\overline{W}$ in the *vicinity* of some $\overline{W}_0$ previously identified. This typically allows to linearize the equations around $\overline{W}_0$. This would make the original procedure (33)–(34) convex with respect to $\overline{W}$, without the need to transform it into the procedure (33)–(35). This is also particularly advantageous in the context of (45), which, as such, is a nonconvex problem and for which it is unclear how to introduce a "convexification reformulation" in the spirit of (35). Under the assumption that we only look for the best $\overline{W}$ in the vicinity of some $\overline{W}_0$, the formulation (45) becomes convex as well, and is thus expected to become much easier to solve.

In all the above contexts, which are very relevant from a practical viewpoint, an interesting question to investigate is how to adapt our approach, in order for instance to be able to recover a reasonably accurate approximation of the effective coefficients at the large scales.

5 Multiscale reaction-diffusion problems

We describe here ongoing works concerned with multiscale reaction-diffusion problems. These works have been performed within the PhD of Alberic Lefort, who joined the team in Fall 2022 (see [L-PhD]), and whose PhD fellowship is partly funded by this EOARD contract.

We consider the following multiscale time-dependent reaction-diffusion problem:

$$\frac{\partial u_\varepsilon}{\partial t} + \frac{1}{\varepsilon^2}\sigma_\varepsilon(x)u_\varepsilon - \operatorname{div}\left(D_\varepsilon(x)\nabla u_\varepsilon\right) = 0 \quad \text{in } (0,T)\times\Omega, \tag{46}$$

where Ω is a bounded domain of $\mathbb{R}^d$ and $T > 0$ is a given final time. The unknown function u_ε is a scalar-valued function defined on $(0,T)\times\Omega$. We complement (46) by homogeneous Dirichlet boundary conditions and an initial condition. This problem appears in several applied fields (as explained below), and it is different from the equations we have studied in the previous funding periods by the fact that it is *time-dependent* and that it includes a *reaction term* (in addition to the diffusive term).

We are interested in the case when the (scalar-valued) reaction coefficient σ_ε and/or the (matrix-valued) diffusion coefficient D_ε are multiscale, i.e. oscillate (in space) at a small scale ε. Our aim is to build an efficient numerical strategy to approximate the solution to (46). Two difficulties are present:

- First, the coefficients of the equation (and therefore the solution u_ε) oscillate at a small spacial scale. Standard discretization approaches (such as finite elements) would need to use a mesh of a small size to obtain an accurate solution, which may be computationally prohibitive. This motivates the use of dedicated numerical approaches (such as the Multiscale Finite Element Method) to capture these spacial oscillations.

- Second, the problem in time is stiff: a standard marching scheme such as the backward Euler scheme would need a small time-step to provide an accurate solution.

In our previous report [EOARD-2022], we have considered this problem from a theoretical perspective, and we have established its homogenized limit, in the periodic setting. We here consider it from a numerical perspective. In order to not address the two difficulties mentioned above at the same time, we are going to consider the following multiscale reaction-diffusion eigenvalue problem:

$$\frac{1}{\varepsilon^2}\,\sigma_\varepsilon(x)\,u_\varepsilon - \operatorname{div}\left(D_\varepsilon(x)\nabla u_\varepsilon\right) = \frac{\lambda_1^\varepsilon}{\varepsilon^2}\,u_\varepsilon \ \text{ in } \Omega, \qquad u_\varepsilon = 0 \ \text{ on } \partial\Omega. \tag{47}$$

We thus look for the *first* eigenvalue of the operator, and its associated eigenfunction (that we assume to be normalized in the sense that $\|u_\varepsilon\|_{L^2(\Omega)} = 1$). Note that, even in that setting, the problem is different from the equations we have studied in the previous funding periods by the fact that it is a *eigenvalue* problem and that it includes a *reaction term* (in addition to the diffusive term). The motivation for considering (47) is threefold:

- This problem can be considered as a first step towards the corresponding time-dependent version (46) of the problem. It is indeed well-known that, to (theoretically and numerically) study linear time-dependent problems of the form $\partial_t u + \mathcal{L}u = 0$, it is useful to first study the eigenmodes of the operator $\mathcal{L}$, i.e. identify (u_j, λ_j) such that $\mathcal{L}u_j = \lambda_j\, u_j$. The solution to the time-dependent problem may indeed by written (at least formally) as $u(t,x) = \sum_j \alpha_j\, \exp(-\lambda_j\, t)\, u_j(x)$ for some coefficients α_j depending on the initial condition.

- Problem (47) only includes the first difficulty mentioned above, namely oscillations at a small spacial scale. We can focus on these, and leave for future works the design of methods to address the fact that the problem (46) is in addition stiff in time.

- Problem (47) appears in several applied fields (and is thus interesting in its own right), including neutronic, which motivates the particular scaling in $1/\varepsilon^2$ of the reaction term. In that case, u_ε represents the neutron density in the system. Generalizations of (47) include vectorial variants of the equation, where each component of u_ε represents the density of neutrons having a certain kinetic energy (the number of possible kinetic energies being finite). We refer e.g. to [2], and also [3, 5, 8, 12, 17].

Our aim here is to build an efficient numerical strategy, in the vein of MsFEM approaches, to approximate the solution to (47). In order to get a better understanding of the problem, we first recall in Section 5.1 its homogenized limit, in the periodic setting. This preliminary step is useful to design numerical approaches, since it provides a description of the main features of the exact solution, a knowledge that guides the choice of discretization methods in order to capture these features. It is indeed well-known that MsFEM methods (briefly presented in Section 3.1) are intimately linked with homogenization. In Section 5.2, we next introduce, in the one-dimensional setting, several variants of multiscale finite element methods and present the numerical results that we have obtained. The multi-dimensional setting is next considered in Section 5.3. We collect in Section 5.4 some perspectives.

5.1 Homogenized limit

In this section, we consider (47) in the periodic setting, and recall its homogenized limit, as established in [2]. Denoting $Y = (0,1)^d$ the periodic cell, the oscillatory equation we study reads as (47) with $\sigma_\varepsilon(x) = \sigma(x/\varepsilon)$ and $D_\varepsilon(x) = D(x/\varepsilon)$, where σ and D are Y-periodic functions. We assume that the matrix D is symmetric and that there exists $\beta \geq \alpha > 0$ such that, for any $\xi \in \mathbb{R}^d$,

$$\forall y \in Y, \quad \alpha \left|\xi\right|^2 \leq \xi^T D(y) \xi \leq \beta \left|\xi\right|^2 \quad \text{and} \quad \alpha \leq \sigma(y) \leq \beta.$$

Consider the smallest eigenvalue μ_1 (and the associated eigenvector ψ, assumed to be normalized by $\|\psi\|_{L^2(Y)} = 1$) of the eigenproblem

$$\sigma\, \psi - \operatorname{div}\left(D \nabla \psi\right) = \mu_1\, \psi, \qquad \psi \text{ is } Y\text{-periodic}.$$

Using the Krein-Rutman theorem, one can show that the smallest eigenvalue μ_1 is simple and that it is possible to choose the eigenvector such that $\psi(y) \geq 0$ (see e.g. [1]).

Consider now, for any $1 \leq i \leq d$, the corrector problem

$$-\operatorname{div}\left(D\, \psi^2 (e_i + \nabla w_i)\right) = 0, \qquad w_i \text{ is } Y\text{-periodic}, \tag{48}$$

and the homogenized matrix $D^\star$ defined by

$$\left[D^\star\right]_{ij} = \int_Y e_i^T D\, \psi^2 \left(e_j + \nabla w_j\right). \tag{49}$$

Consider next the smallest eigenvalue ν_1 (and the associated eigenvector v, again satisfying $\|v\|_{L^2(\Omega)} = 1$) of the eigenproblem

$$-\operatorname{div}\left(D^\star \nabla v\right) = \nu_1\, v \ \text{ in } \Omega, \qquad v = 0 \ \text{ on } \partial\Omega. \tag{50}$$

It is shown in [2] that

$$\lim_{\varepsilon \to 0} \left\| \frac{u_\varepsilon(x)}{\psi(x/\varepsilon)} - \left(v(x) + \varepsilon \sum_{i=1}^d w_i\left(\frac{x}{\varepsilon}\right) \frac{\partial v}{\partial x_i}(x) \right) \right\|_{H^1(\Omega)} = 0. \tag{51}$$

The proof of this result actually goes by observing that the function v_ε defined by $v_\varepsilon(x) = \dfrac{u_\varepsilon(x)}{\psi(x/\varepsilon)}$ is the solution to the following (generalized) multiscale eigenvalue problem: find the smallest eigenvalue ν_1^ε and the associated eigenfunction v_ε such that

$$-\operatorname{div}\left(D_\varepsilon\, \psi_\varepsilon^2\, \nabla v_\varepsilon\right) = \nu_1^\varepsilon\, \psi_\varepsilon^2\, v_\varepsilon \ \text{ in } \Omega, \qquad v_\varepsilon = 0 \ \text{ on } \partial\Omega, \tag{52}$$

where $\psi_\varepsilon = \psi(\cdot/\varepsilon)$. This eigenvalue problem involves only a diffusion operator (in contrast to (47) which includes a large reaction term). Its homogenized limit can be identified using standard homogenization tools (such as, formally, a two-scale ansatz). This leads to the introduction of the corrector problems (48), of the homogenized matrix $D^\star$ defined by (49), and of the homogenized eigenvalue problem (50). Note that the function ψ^2, present in the right-hand side of the oscillatory problem (52), only affects the right-hand side of the homogenized problem (50) through its average, which is equal to 1 in view of the fact that ψ is periodic and $\|\psi\|_{L^2(Y)} = 1$.

The smallest eigenvalues ν_1^ε and ν_1 being simple, we have that ν_1^ε converges to ν_1 and v_ε converges (strongly in $L^2(\Omega)$, weakly in $H^1(\Omega)$) to $\pm v$ when ε goes to 0. Furthermore, denoting by $+v$ the limit of v_ε, the difference $v_\varepsilon - \left(v + \varepsilon \sum_{i=1}^{d} w_i(\cdot/\varepsilon)\, \partial_i v \right)$ goes to 0 strongly in $H^1(\Omega)$ when $\varepsilon \to 0$, which is exactly the claim (51).

5.2 MsFEM approaches: the one-dimensional case

We now restrict ourselves to the one-dimensional setting, set $\Omega = (0,1)$, and introduce a uniform coarse mesh (with elements of size H) of Ω, the interior nodes of which are denoted x_j, $1 \le j \le N_v$. We return to the general notation D_ε and σ_ε.

5.2.1 A preliminary, non-operational MsFEM approach

To start with, we temporarily *assume* that we have at our disposal the function ψ, and denote ψ_ε the function defined by $\psi_\varepsilon(x) = \psi(x/\varepsilon)$ (of course, in practice, we do not have this function ψ_ε at hand and we will have to actually determine an approximation of it, a task we will achieve in Section 5.2.2 below). For each node i of the mesh, we introduce the function χ_i^ε, solution on each mesh element to the problem

$$-\operatorname{div}\left(D_\varepsilon\, \psi_\varepsilon^2\, \nabla \chi_i^\varepsilon\right) = 0$$

with the boundary conditions $\chi_i^\varepsilon(x_j) = \delta_{ij}$. Our intuition is that v_ε solution to (52) should be well-approximated in the space $\operatorname{Span}\{\chi_i^\varepsilon,\ 1 \le i \le N_v\}$. In view of the relation $u_\varepsilon = \psi_\varepsilon\, v_\varepsilon$, we next consider the multiscale approximation space

$$V_H^\varepsilon = \operatorname{Span}\left\{\psi_\varepsilon\, \chi_i^\varepsilon,\ 1 \le i \le N_v\right\},$$

and define the MsFEM solution using a Galerkin approximation of (47) on the space V_H^ε: we look for the first eigenvalue $\lambda_1^{H,\varepsilon}$ and its associated eigenfunction $u_H^\varepsilon \in V_H^\varepsilon$

such that

$$\forall v \in V_H^\varepsilon, \qquad \frac{1}{\varepsilon^2}\int_\Omega \sigma_\varepsilon\, u_H^\varepsilon\, v + \int_\Omega \nabla v \cdot D_\varepsilon \nabla u_H^\varepsilon = \frac{\lambda_1^{H,\varepsilon}}{\varepsilon^2}\int_\Omega u_H^\varepsilon\, v. \tag{53}$$

We have investigated the performance of this preliminary MsFEM approach in a periodic case, in order to start with a simple situation. We thus set

$$\sigma_\varepsilon(x) = \sigma(x/\varepsilon) \qquad \text{and} \qquad D_\varepsilon(x) = D(x/\varepsilon) \tag{54}$$

with

$$\sigma(x) = 20\,(2+\sin(2\pi x)) \qquad \text{and} \qquad D(x) = 6 + 5\sin(2\pi x), \tag{55}$$

with $\varepsilon = 0.002$. We monitor the accuracy, defined as the relative error

$$\mathrm{Err}_{\mathrm{relative}} = \frac{\|\nabla u_H^\varepsilon - \nabla u_\varepsilon\|_{L^2(\Omega)}}{\|\nabla u_\varepsilon\|_{L^2(\Omega)}}, \tag{56}$$

as a function of the coarse mesh size H. Results are shown on Figure 9. For the sake of comparison, we also plot on that figure the results obtained using a standard P1 approach on the coarse mesh.

We observe that the preliminary method provides very accurate results. For all the values of H we have considered, the relative error (56) is smaller than 3%. As expected, the P1 approach accuracy is poor (with errors of the order of 100%). Our aim in the next section is to introduce an accurate approximation of ψ_ε, a function that we do not know in practice (and which is not defined in a non-periodic context), in order to practically mimick this preliminary method.

5.2.2 A practical MsFEM approach

We introduce the following approximation ϕ_ε of ψ_ε. For each element $K_j = [jH, (j+1)H]$ of the coarse mesh, we consider an oversampling extension $S_j = [(j-1)H, (j+2)H]$. On each element S_j, we solve an eigenvalue problem: we look for the first eigenvalue $\mu_{1,j}^{H,\varepsilon}$ and its associated eigenfunction $\Phi_j^{H,\varepsilon} \in H_0^1(S_j)$ solution to

$$\frac{1}{\varepsilon^2}\,\sigma_\varepsilon(x)\,\Phi_j^{H,\varepsilon} - \mathrm{div}\left(D_\varepsilon(x)\nabla\Phi_j^{H,\varepsilon}\right) = \frac{\mu_{1,j}^{H,\varepsilon}}{\varepsilon^2}\,\Phi_j^{H,\varepsilon} \ \text{ in } S_j, \qquad \Phi_j^{H,\varepsilon} = 0 \ \text{ on } \partial S_j.$$

We next introduce the function ϕ_ε defined on Ω by

$$\forall 1 \le j \le N_v, \qquad \forall x \in K_j, \qquad \phi_\varepsilon(x) = \Phi_j^{H,\varepsilon}(x).$$

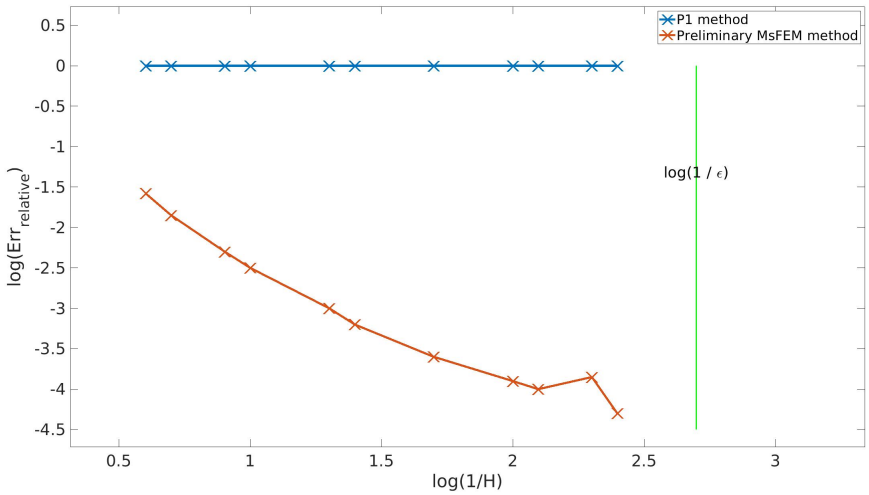

Figure 9 – Accuracy (quantified by (56)) of the preliminary MsFEM approach (in log-log plot) as a function of H, for $\varepsilon = 0.002$ (1D case). The vertical green line is drawn for the value $H = \varepsilon$. The regime of interest for MsFEM is $H \geq \varepsilon$, hence the part of the plot on the left-hand side of that green line.

Note that the function ϕ_ε is (in general) not continuous at the node vertices.

We next proceed similarly as in the approach described in Section 5.2.1, replacing everywhere ψ_ε by ϕ_ε. For each node i of the mesh, we thus introduce the function χ_i^ε, solution on each mesh element of

$$-\operatorname{div}\left(D_\varepsilon\, \phi_\varepsilon^2\, \nabla \chi_i^\varepsilon\right) = 0$$

with the boundary conditions $\chi_i^\varepsilon(x_j) = \delta_{ij}$. We next consider the multiscale approximation space

$$V_H^\varepsilon = \operatorname{Span}\left\{\phi_\varepsilon\, \chi_i^\varepsilon,\ 1 \leq i \leq N_v\right\}, \tag{57}$$

and define the MsFEM solution u_H^ε using the Galerkin approximation (53) of (47) on the space V_H^ε defined by (57).

We investigate the performance of that practical MsFEM approach for the same test case as above (see (54)–(55), where we again fix $\varepsilon = 0.002$). The relative error (defined by (56)) of both the preliminary and the practical MsFEM approaches are shown on Figure 10 as a function of the coarse mesh size H.

We observe that the practical method that we have just introduced is not as accurate as the preliminary method of Section 5.2.1, but that it already provides en-

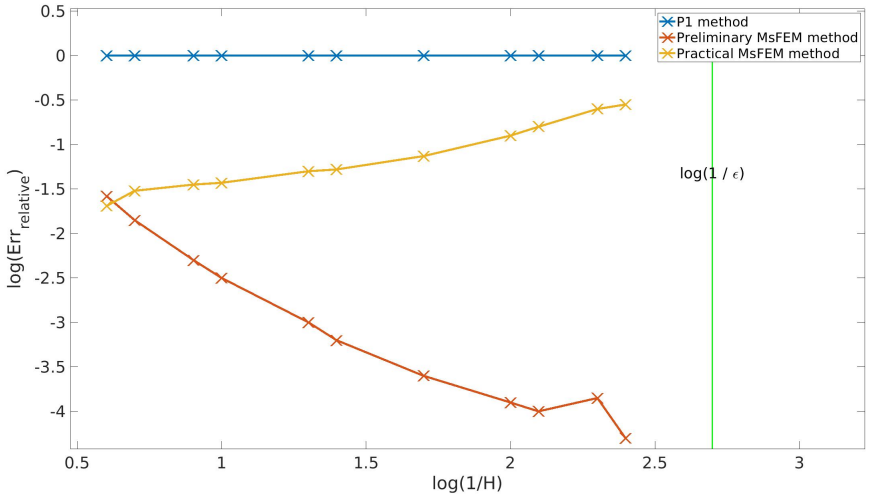

Figure 10 – Accuracy (quantified by (56)) of the MsFEM approaches (in log-log plot) as a function of H, for $\varepsilon = 0.002$ (1D case). As in Figure 9, the vertical green line is drawn for the value $H = \varepsilon$.

couraging results (with errors between 3 and 10%) when H is sufficiently larger than ε.

5.3 MsFEM approaches: the two-dimensional case

We now consider a two-dimensional setting and set $\Omega = (0,1)^2$. We consider a structured mesh of Ω made of squares of size $H \times H$ that we next cut in half in order to obtain a triangular mesh $\mathcal{T}_H$. In order to mimick the oversampling procedure considered in Section 5.2.2, we embed each triangular element K_j of $\mathcal{T}_H$ into a oversampling square S_j of size $2H \times 2H$, on which we solve an eigenvalue problem: we look for the first eigenvalue $\mu_{1,j}^{H,\varepsilon}$ and its associated eigenfunction $\Phi_j^{H,\varepsilon} \in H^1(S_j)$ solution to

$$\frac{1}{\varepsilon^2}\,\sigma_\varepsilon(x)\,\Phi_j^{H,\varepsilon} - \mathrm{div}\left(D_\varepsilon(x)\nabla\Phi_j^{H,\varepsilon}\right) = \frac{\mu_{1,j}^{H,\varepsilon}}{\varepsilon^2}\,\Phi_j^{H,\varepsilon} \quad \text{in } S_j, \tag{58}$$

with periodic boundary conditions on the boundary of S_j. We next introduce the function ϕ_ε defined on $\Omega = \cup_j K_j$ by

$$\forall x \in K_j, \qquad \phi_\varepsilon(x) = \Phi_j^{H,\varepsilon}(x).$$

Note that, as in the one-dimensional case, the function ϕ_ε is (in general) not continuous across the edges of the mesh. We next proceed similarly as in the approach described in Section 5.2.2. For each node i of the mesh, we thus introduce the function χ_i^ε, solution on each mesh element of

$$-\operatorname{div}\left(D_\varepsilon\,\phi_\varepsilon^2\,\nabla\chi_i^\varepsilon\right)=0 \tag{59}$$

with the boundary conditions $\chi_i^\varepsilon=\chi_i^0$, where χ_i^0 is the $\mathbb{P}_1$ basis function associated to the vertex i of $\mathcal{T}_H$. We next consider the multiscale approximation space V_H^ε defined by (57) and define the MsFEM solution u_H^ε using the Galerkin approximation (53) on the space V_H^ε defined by (57).

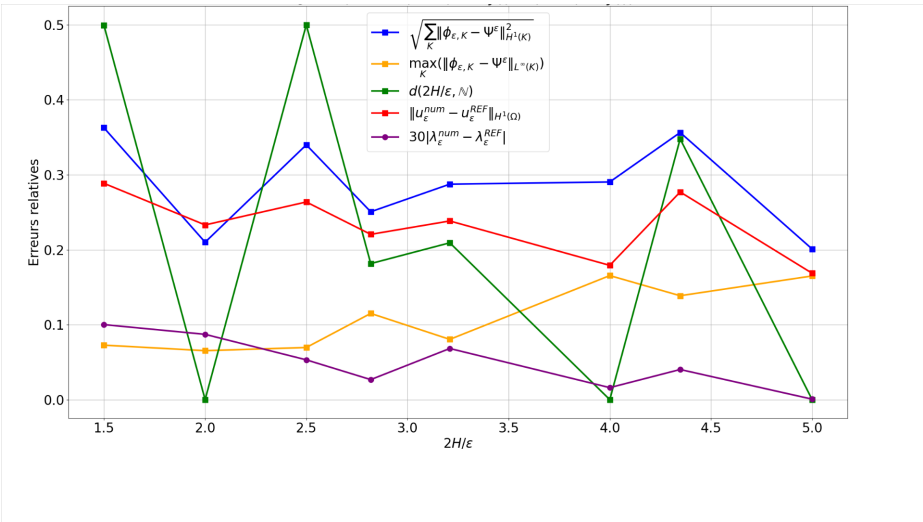

Figure 11 – Red and purple curves: accuracy of the practical MsFEM approach for different values of ε (2D case, $H=1/8$). The other curves monitor the accuracy of intermediate quantities, as explained in the text.

Numerical results are shown on Figure 11 in the periodic case, for the coefficients σ_ε and D_ε given by (54) with

$$\sigma(x)=20\left(2+\cos\left(2\pi(x_1-2x_2)\right)\sin\left(2\pi(x_1-x_2)\right)\right),$$
$$D(x)=6+5\cos\left(2\pi(x_1+2x_2)\right)\sin\left(2\pi(x_1-x_2)\right).$$

The axis of symmetry of σ and D are deliberately not aligned (but rather tilted) with the vertical and horizontal axis of the mesh. We fix $H=1/8$ (and $h=1/1024$ for

the computation of the basis functions and of the reference solution denoted u_ε^{REF} on Figure 11) and consider several values of ε. When moving to the right-hand side of Figure 11, the value of ε decreases, which means that the offline stage becomes more expensive (the cost of the online stage is the same for all points of the figure, since it essentially only depends on H).

The green curve of Figure 11 shows the distance between $2H/\varepsilon$ and the closest integer. It is a measure of how well $2H$ can be considered as a multiple of ε. If that distance vanishes, then each oversampling square S_j (the size of which, we recall, is $2H \times 2H$) exactly contains an integer number of periods, which is a very particular situation. The generic situation is when S_j does not contain an integer number of periods, which is for instance the case when the distance between $2H/\varepsilon$ and the closest integer reaches its maximum, namely $1/2$.

The blue and yellow curves of Figure 11 investigate (in the relative broken $H^1(\Omega)$ norm and in the relative L^∞ norm, respectively) how well the practical function ϕ_ε approximates the ideal function ψ_ε. We see that the error is of the order of 30% in the broken $H^1(\Omega)$ norm, and of the order of 10% in the L^∞ norm.

We eventually monitor the accuracy of the MsFEM solution (denoted u_ε^{num} on Figure 11), by computing the relative broken H^1 error (shown in red) between the eigenfunctions, defined by

$$\frac{\sqrt{\sum_K \|u_\varepsilon^{num} - u_\varepsilon^{REF}\|^2_{H^1(K)}}}{\|u_\varepsilon^{REF}\|_{H^1(\Omega)}},$$

and the relative error (shown in purple) between the eigenvalues. Since the latter quantity turns out to be much smaller than the other ones, we actually plot (for the sake of visibility) the ratio

$$30\,\frac{|\lambda_\varepsilon^{num} - \lambda_\varepsilon^{REF}|}{|\lambda_\varepsilon^{REF}|}$$

rather than $|\lambda_\varepsilon^{num} - \lambda_\varepsilon^{REF}|/|\lambda_\varepsilon^{REF}|$ on Figure 11. We observe that the error on the eigenfunction is of the order 20 to 30 %, which is a very encouraging first result. The error on the eigenvalue is much smaller (as is often the case for eigenproblems), and is of the order of 1% or less. Our temporary conclusion (which is of course yet to be confirmed) is that the practical MsFEM method we have introduced yields a fairly accurate approximation (for all practical purposes) of the exact solution.

5.4 Perspectives

The numerical results obtained so far are very encouraging. We wish to pursue this work in the following directions:

- investigate the robustness of our approach, by considering other test cases, including *non-periodic* ones. The influence of the contrast (in D_ε and in σ_ε) needs also to be understood.

- in order to better understand the behavior of the approach, it is interesting to consider an alternative method, where we again solve (58) on the oversampling domain S_j, but now complemented by homogeneous Dirichlet boundary conditions. Such a test should help us understand whether the results are sensitive to the precise boundary conditions set on ∂S_j.

- investigate how our approach can be extended to approximate the other eigenmodes of (47), besides the first one studied here. Our motivation is two-fold. First, multiscale numerical approaches are particularly efficient (in terms of computational cost) in multi-query contexts. Approximating several eigenmodes is one such context, where we may hope to perform only once the offline stage (that is, solving for the fundamental eigenmode (58) and the associated functions χ_i^ε defined by (59)) and to use the obtained multiscale approximation space V_H^ε to compute, in the online stage, many eigenmodes. A second motivation is the fact that the eigenproblem (47) can be considered as a first step toward the time-dependent problem (46). In that perspective, all the eigenmodes of (47) matter from a theoretical perspective. From a numerical perspective, it is not required to compute *all eigenmodes*, but we definitely need more than simply the very first eigenmode.

- return to the time-dependent setting and approximate (46). The MsFEM discretization space is expected to accurately capture the oscillations in space, and we are thus left with the stiffness in time difficulty.

We hope to proceed in these directions in the context of a renewed funding.

References[4]

[1] G. Allaire, Dispersive limits in the homogenization of the wave equation, *Annales de la Faculté des sciences de Toulouse: Mathématiques*, 12(4):415–431, 2003.

[2] G. Allaire and Y. Capdeboscq, Homogenization of a spectral problem in neutronic multigroup diffusion, *Comput. Methods Appl. Mech. Engrg.*, 187:91–117, 2000.

[3] G. Allaire and F. Malige, Spectral asymptotic analysis of a neutronic diffusion problem, *C. R. Acad. Sci. Paris, Série I*, 324:939–944, 1997.

[4] A. Bensoussan, J.-L. Lions and G. Papanicolaou, *Asymptotic analysis for periodic structures*, Studies in Mathematics and its Applications, vol. 5, North-Holland 1978.

[5] Y. Capdeboscq, Homogenization of a neutronic critical diffusion problem with drift, *Proc. Royal Soc. Edinburgh: Section A Math.*, 132(3):567–594, 2002.

[6] A.-L. Dalibard, Homogenization of a quasilinear parabolic equation with vanishing viscosity, *J. Math. Pures Appl.*, 86:133–154, 2006.

[7] B. Després, Quadratic stability of flux limiters, *Math. Model. Numer. Anal.*, 57:395–422, 2023.

[8] K. Dugan, R. Sanchez and I. Zmijarevic, Cross section homogenization for transient calculations in a spatially heterogeneous geometry, *Annals of Nuclear Energy*, 116:439–447, 2018.

[9] Y. Efendiev and T.Y. Hou, *Multiscale Finite Element Methods*, Surveys and Tutorials in the Applied Mathematical Sciences, vol. 4, Springer, 2009.

[10] T.Y. Hou and X.-H Wu, A Multiscale Finite Element Method for elliptic problems in composite materials and porous media, *J. Comput. Phys.*, 134(1):169–189, 1997.

[11] P. Jenny, S.H. Lee and H.A. Tchelepi, Multi-scale finite-volume method for elliptic problems in subsurface flow simulation, *J. Comput. Phys.*, 187:47–67, 2003.

[4] We collect here general references and references authored by the investigators and not related to the contract. References authored by the investigators (and their students) in the context of the contract are listed in the Executive Summary.

[12] E.W. Larsen and R.P. Hughes, Homogenized diffusion approximations to the neutron transport equation, *Nuc. Science Eng.*, 73:274–285, 1980.

[13] C. Le Bris and F. Legoll, Examples of computational approaches for elliptic, possibly multiscale PDEs with random inputs, *J. Comput. Phys.*, 328:455–473, 2017.

[14] C. Le Bris, F. Legoll and S. Lemaire, On the best constant matrix approximating an oscillatory matrix-valued coefficient in divergence-form operators, *Control, Optimisation and Calculus of Variations*, 24(4):1345–1380, 2018.

[15] C. Le Bris, F. Legoll and K. Li, Coarse approximation of an elliptic problem with highly oscillatory coefficients, *C. R. Acad. Sci. Paris, Série I*, 351(7-8):265–270, 2013.

[16] C. Le Bris, F. Legoll and F. Madiot, A numerical comparison of some Multiscale Finite Element approaches for advection-dominated problems in heterogeneous media, *Math. Model. Numer. Anal.*, 51(3):851–888, 2017.

[17] Z. Woznicki, The numerical analysis of eigenvalue problem solutions in the multigroup neutron diffusion theory, *Prog. Nuc. Energy*, 33(3):301–391, 1998.